EBM Experimental Biology and Medicine

TYPE Original Research
PUBLISHED 05 March 2026
DOI 10.3389/ebm.2026.10867

OPEN ACCESS

*CORRESPONDENCE
Mmei Cheryl Motshudi,
cheryl.motshudi@smu.ac.za

RECEIVED 19 October 2025
REVISED 10 January 2026
ACCEPTED 16 February 2026
PUBLISHED 05 March 2026

CITATION
Motshudi MC, Naidoo CM, Obi CL, Iweriebor BC, Prinsloo E, Zubair MS and Mkolo NM (2026) Metabolomics-guided identification of bioactive phytometabolites from South African plants targeting neuroblastoma. *Exp. Biol. Med.* 251:10867. doi: 10.3389/ebm.2026.10867

Metabolomics-guided identification of bioactive phytometabolites from South African plants targeting neuroblastoma

Mmei Cheryl Motshudi[1]*, Clarissa Marcelle Naidoo[1], Chikwelu Lawrence Obi[1], Benson Chucks Iweriebor[1], Earl Prinsloo[2], Muhammad Sulaiman Zubair[3] and Nqobile Monate Mkolo[1]

[1]Department of Biology, School of Science and Technology, Sefako Makgatho Health Science University, Pretoria, South Africa, [2]Department of Biotechnology, Rhodes University, Makhanda, South Africa, [3]Department of Pharmacy, University of Tadulako, Palu, Indonesia

Abstract

Neuroblastoma constitutes a solid tumor in pediatric populations, characterized by a dismal prognosis and a scarcity of effective therapeutic interventions. Medicinal flora from South Africa represents valuable sources of bioactive phytometabolites with potential relevance to neuroblastoma. This study employed an integrated workflow merging untargeted UPLC-MS/MS metabolomics, mitochondrial functional assays, and *in silico* absorption, distribution, metabolism, and excretion (ADME) prediction to systematically identify bioactive metabolites from *Acorus calamus* and *Lippia javanica* with activity against SH-SY5Y neuroblastoma cells. Cytotoxic effects were quantified utilizing the CCK-8 assay, while mitochondrial membrane potential ($\Delta\Psi m$) was conducted through JC-1 flow cytometry. Untargeted UPLC-MS/MS profiling yielded metabolomic fingerprints, through PCA, PLS-DA, and OPLS-DA. ADME and drug-likeness were predicted using SWISSADME. Both plant extracts exhibited dose-dependent inhibition of SH-SY5Y cell viability, with IC_{50} values determined at 0.2886 µg/µL for *A. calamus* and 0.3066 µg/µL for *L. javanica*. The $\Delta\Psi m$ assessment indicated enhanced mitochondrial polarization (68.2% and 65.4% compared to 58.8% in untreated controls), implying modulation of mitochondrial functional status. Metabolomic profiling unveiled distinct phytochemical signatures, including flavonoids, phenolics, jasmonates, and alkaloids, exhibiting significant species-level differentiation (F = 936.71, R^2 = 0.989, p = 0.005). Notable metabolites such as isopropyl β-glucoside, 6β-hydroxymethandienone, and 7-epi-12-hydroxyjasmonic acid demonstrated favorable ADME characteristics and permeability across the blood-brain barrier. This investigation elucidates that *A. calamus* and *L. javanica* possess

potential efficacy against neuroblastoma, underscoring the translational potential of African medicinal flora in pediatric oncology and necessitating further preclinical exploration.

KEYWORDS

Acorus calamus, ADME, *Lippia javanica*, metabolomics, mitochondrial membrane potential

Impact statement

This manuscript serves to investigate the medicinal flora for natural bioactive compounds as probable sources of therapeutic anticancer agents targeting SH-SY5Y neuroblastoma cells. Utilizing a multifaceted methodology that incorporates cytotoxicity assays, untargeted metabolomics, and in silico Absorption, Distribution, Metabolism, and Excretion modeling, we have identified phytometabolites exhibiting promising anticancer efficacy and have also predicted their permeability across the blood–brain barrier. The findings will offer different perspectives and insights into the metabolomic profiling and therapeutic potential of the medicinal plants, thereby enhancing the pharmacological comprehension of phytochemical agents in pediatric oncology.

This manuscript also highlights the current strategic plans for neuroblastoma treatment and approaches that could be applied in the future to improve the quality of life of patients with neuroblastoma, as well as to provide early diagnostic measures to reduce mortality rates of this fatal cancer. This information could be of great use for both clinical and scientific research.

Introduction

Neuroblastoma (NB) is a primary cancer detected in infants; it is a predominant solid tumor commonly found in the extracranial area in children [1]. Neuroblastoma accounts for approximately 10–15% of childhood malignancies, and the primary tumour generally stems from the sympathetic chain, usually in the abdomen or in the adrenal gland [2]. Patients with neuroblastoma tend to exhibit a wide range of biological, clinical, accompanied by prognostic heterogeneity, and a fundamental prognostic trait pertaining to neuroblastoma patients is the location of the primary tumour, which can originate in the adrenal gland, abdominal/retroperitoneal area, neck, thorax, pelvis, or, less frequently, in other sites [3, 4]. Due to the heterogeneous biological nature of neuroblastoma, its prognosis, along with clinical course, differs between spontaneous regression to high-risk cases, with several neuroblastoma tumours exhibit poorly responsive to intensive multimodal therapy [5, 6]. Presently treatment strategies involve aggressive amalgamation of radiotherapy, induction chemotherapy, elevated-dose chemotherapy with autologous stem-cell rescue, surgical removal of tumors, and applications of post-consolidation methods such as immunotherapy, as well as differentiation therapy [7]. The 5-year overall survival rate for high-risk neuroblastoma individuals continues to hover around 50–60% despite these integrated multimodal approaches, and late effects are usually imminent and frequently experienced by long-term survivors [8]. Regardless of advancement in multimodal therapy, outcomes for high-risk neuroblastoma persist to be suboptimal, highlighting the necessity for alternative and complementary therapeutic strategies.

The SH-SY5Y human neuroblastoma cell line comprises an N-type catecholaminergic subclone of neuroblastoma commonly used in research areas pertaining to neuroblastoma and neurobiology [9]. SH-SY5Y cell lines convey crucial elements of human catecholaminergic systems, which encompass components such as dopamine-β-hydroxylase and tyrosine hydroxylase [10]. Induced SHSY5Y cells can be differentiated into phenotypes that resemble neurons, therefore rendering them an adaptable *in vitro* model [11]. However, limitations such as inadequate maturation levels of neurons and restricted functionality of network systems, irrespective of the differentiation, emphasize the necessity of cautious interpretation of pharmacological responses [12]. Changes in mitochondrial membrane potential ($\Delta\Psi m$) and cellular redox balance can play context-dependent roles in cancer biology, acting as regulators of cell survival and cell death conditional on cellular state and therapeutic pressure [13]. Although moderate stabilization of mitochondrial function and redox homeostasis might permit tumour cell adaptation, excessive or dysregulated perturbation of these pathways can encourage cytotoxic or cytostatic outcomes via mitochondrial dysfunction [14, 15]. Accordingly, modulation of $\Delta\Psi m$ and redox-related processes has been explored as a functional vulnerability in cancer cells, also neuroblastoma, instead as a unidirectional pro-survival mechanism [16, 17].

Approximately 65% of the world's population, along with an estimated 80% of the population in Africa as well as Asia, depends on traditional herbal remedies to cure and furthermore prevent infectious ailments and chronic diseases [18, 19]. Ethnobotanical knowledge from southern Africa has showcased many species of aromatic origin known for their anticancer, anti-inflammatory, and anti-infective properties [20]. South African based medicinal plants are rich sources of structurally diverse phytometabolites with documented biological activities, and systematic investigation of these resources might permit the discovery of candidate anti-cancer

chemotypes or complementary approaches to present therapies [21–25]. *Lippia javanica* (Burm.f.) is a multi-branched woody shrub, that is commonly known as fever tea [9, 26]. *L. javanica* (Verbenaceae family) is an aromatic medicinal plant indigenous to eastern and southern Africa that has been broadly explored for its phytochemical composition and biological activities [26–30]. Previous studies have recognized phenolic, terpenoids, and flavonoids constituents, with apigenin- and luteolin-associated derivatives, which *in vitro* exhibit antioxidant and cytotoxic activities, supporting its importance for further assessment within a metabolomics-directed anticancer framework [31–36]. *Acorus calamus* Linn., (Aceraceae family), is classified as a perennial, semi-aquatic herb, that is commonly known as sweet flag {25]. *A. calamus* is an aromatic medicinal plant that has been extensively studied for its phytochemical diversity and biological activities, and it is frequently utilized in traditional Chinese and Indian medicine [37–41]. Notably, this plant comprises phenylpropanoid constituents for instance α- and β-asarone, for which extracts and isolated compounds have established anticancer activity in preclinical cancer models, also permitting its inclusion in metabolomics-directed anticancer investigations [42, 43]. Untargeted LC-MS metabolomics is commonly utilized to map systematic methods for enhancing quality control, distinguishing chemotypes, associating chemical properties with bioactivity of samples, and prioritizing key metabolites for further pharmacology analysis, alongside *in silico* ADME assessment through tools like SwissADME and the BOILED-Egg model [44–47].

Building on the above insight, while the phytochemistry and bioactivity of *L. javanica* and *A. calamus* have been previously reported in various biological contexts, their assessment within an integrated framework relating metabolomic composition to mitochondrial functional outcomes and pharmacokinetic possibility remains limited. In this study, we integrated untargeted UPLC-MS/MS metabolomics, mitochondrial membrane potential evaluation in SH-SY5Y neuroblastoma cells, and *in silico* ADME analysis to select metabolites with possible neuroblastoma importance.

Materials and methods

Plant collection and identification

Specimens of *L. javanica* and *A. calamus* were collected from Hartbeespoort in the North-West Province of South Africa (25.7236° S, 27.9653° E) in February 2023. Organ-matched sampling was applied to follow metabolomics reporting recommendations that highlight control of tissue-specific variability in comparative chemical analyses [48]. Species identification of both plants was authenticated by taxonomists at the National Herbarium, where voucher specimens were deposited under accession numbers NR 904 (*L. javanica*) and NR 905 (*A. calamus*). Plant material collection was completed in accordance with national regulatory requirements, under permit CF6-0234 released by the Department of Agriculture and Rural Development-Nature Conservation, South Africa (Permit Holder: Prof. Nqobile Monate Mkolo).

Anti-cancer assay analysis

Sample preparation

The *L. javanica* and *A. calamus* samples were pulverized into a powder using a mortar and pestle under liquid nitrogen. A precise weight of 0.5 g from each powdered sample was combined into a single 50 mL centrifuge tube. A total of 10 mL of buffer was added to the tube followed by extraction at a 4 °C. The extractant was filtered through a 0.45 μm filter, and the clearer supernatants were transferred into a new centrifuge tube. Crude extracts and intermediate preparations were stored at −20 °C in amber, light-protected containers to reduce degradation. Extracts were permitted to equilibrate to room temperature and were used within 1 week of preparation to allow stability and duplicability.

SH-SY5Y cell preparation

Human neuroblastoma SH-SY5Y cells (Cellonex ™, Johannesburg South Africa) were cultured in Dulbecco's Modified Eagle's Medium (DMEM) supplemented with 10% (v/v) heat-inactivated fetal bovine serum, 1% penicillin-streptomycin obtained from Gibco (New York, NY, United States), and maintained at 37 °C in a humidified incubator with 5% CO_2 [49]. Cells were washed by utilizing a 1 mL pipette to aspirate and discard the old medium. Gradually, 2 mL of Phosphate Buffered Saline (PBS) from Sigma-Aldrich (St. Louis, MO, United States), was poured along the edge of the T25 flask, and this flask was gently swirled to wash away any remaining medium. Cell digestion was conducted by gradually adding 1 mL of 0.25% trypsin digest solution (Sigma-Aldrich, St. Louis, MO, United States) into the T25 flask, ensuring it covered all the cells. The flask was then placed in a 37 °C CO_2 incubator for 2 min. Cells were examined, using an inverted microscope, for separation and formation of a spherical shape. To stop digestion, 4 mL of cell growth medium was added to the cells. Passage was done at a ratio of 1:4, where the cells were carefully pipetted for dispensation, and a single-cell suspension was confirmed under the microscope.

CCK-8 assay

The effect of chosen plant tissue (final concentration of 0.01–10 μg/mL) on SH-SY5Y cell viability was assessed using the CCK-8 assay according to the protocol [50]. SH-SY5Y cells were collected from an approximately 80% confluent T-25 flask using the standard trypsinization method. Afterward, 2×10^4

cells were seeded in a 96-well plate and incubated for 24 h at 37 °C. Then, the media was removed, rinsed with PBS, and the cells were treated with 100 μL of clear supernatants from the sample, while the cell medium served as the negative control. Following 24 h, 10 μL of CCK-8 was added to every well and allowed to incubate for 2 h. A microplate reader (Infinite M200, Tecan, Switzerland) scanned the 96-well plate at a wavelength of 450 nm. All CCK-8 experiments were performed utilizing three independent biological replicates, with each condition examined in technical triplicate. The subsequent formula was applied to determine the percentage of cell viability:

$$\text{Survival rate (\%)} = (\text{Asample} - \text{Ab}/\text{Ac} - \text{Ab}) \times 100$$

Wherein Asample, Ab, and Ac are the absorbance/Optical density of cells exposed to test reagents, absorbance/Optical density of blank, and negative control, respectively.

Mitochondrial membrane potential detection

The mitochondrial membrane potential (ΔΨm) of SHSY-5Y cells against *L. javanica* and *A. calamus* was determined by adopting a procedure of Sakamuru and co-workers [51]. SH-SY5Y cells were seeded in a 96-well plate (2×10^4 cells per well) according to experimental groups, which included the blank control group (non-treated SH-SYSY cell line), negative control of non-treated SH-SYSY cell line for gating, and the treated SH-SYSY cell line group (*L. javanica* and *A. calamus* at 1 μg/uL). After 24 h of treatment, the cells were collected using trypsin for adherent cells to avoid over-digestion and to prevent membrane potential damage. A JC-1 working solution was prepared using a diluted JC-1 stock solution with pre-warmed (37 °C) medium, which was added to the final concentration. The JC-1 working solution was then added to the cells and incubated at 37 °C in the dark for 15 min. JC-1 solution was removed, and cells were washed 3 times with pre-cooled PBS to remove unbound dye. The cells were collected using trypsin, then centrifuged and resuspended into PBS. The set flow cytometry channels were green fluorescence, which was the FL1 channel (Ex 488 nm, Em 530/30 nm), and red fluorescence, which was the FL2 channel (Ex 488 nm, Em 585/42 nm). The red fluorescence (normal mitochondria) and green fluorescence (decreased membrane potential) were then merged for analysis. Mitochondrial membrane potential (ΔΨm) assessments were conducted utilizing three independent biological replicates, with technical triplicates for each experimental condition.

Metabolomic characterization

Chemicals and instrumentation

Multiple chemicals and reagents, such as acetonitrile (Merck, Rahway, NJ, United States), methanol (Merck, Rahway, NJ, United States), DL-o-Chlorophenylalanine (Merck, Rahway, NJ, United States), and formic acid (Merck, Rahway, NJ, United States) were utilized. Additionally, instrumentation, namely ACQUITY UPLC HSS T3 (100 × 2.1 mm × 1.8 μm), Ultimate 3000LC combined with Q Exactive MS (Thermo, Waltham, MA, United States), and Temp functional Centrifugation (Eppendorf, Enfield, CT, United States) were utilized.

Sample preparation

The initial stages of the sample preparation comprised a freeze-drying process (lyophilization) of *A. calamus* and *L. javanica* leaf samples. The respective samples were subsequently dried and ground into powder; the resultant powder for each sample was transferred into a 5 mL homogenizing tube. A MM 400 mixer with four 5 mm diameter metal balls was utilized to mix the samples at 30 Hz. The subsequent product for each sample was added with 80% methanol at a volume of 800 μL. The resultant solution was vortexed for 30 s and sonicated thereafter for 30 min at 4 °C. Samples were stored at a temperature of −20 °C for an hour. Each sample was centrifuged thereafter at 12,000 rpm, 4 °C for 5 min. A total of 200 μL of each supernatant from the respective samples, along with 5 μL of DL-o-Chlorophenylalanine (140 μg/mL), were added to vials. The vials were then used for liquid chromatography–mass spectroscopy (LC-MS) analysis.

Untargeted plant metabolomics analysis using UPLC-MS/MS

Separation of compounds was carried out using the Ultimate 3000LC (Thermo, Waltham, MA, United States) combined with QExactive MS (Thermo) and additionally, screened with ESI-MS [27]. The first solvent of the mobile phase comprised 0.05% formic acid in water and the second solvent was acetonitrile with a subsequent gradient elution (0–1 min, 95% A; 1–12 min, 95%–5% A; 12–13.5 min, 5% A; 13.5–13.6 min, 5–95% A; 13.6–16 min, 95% A). The mobile phase had a flow rate of 0.3 mL·min^{-1}. The column temperature was kept at 40 °C, while the sample manager temperature was adjusted to 4 °C. The mass spectrometry settings for electrospray ionization ESI+ mode are detailed as follows: heater temperature 300 °C; sheath gas flow rate, 45 arb; auxiliary gas flow rate, 15 arb; sweep gas flow rate, 1 arb; spray voltage, 3.0 kV; capillary temperature, 350 °C; S-Lens RF level, 30%.

Quality control samples

Extracts of the respective plants were mixed as quality control samples (QC) to evaluate the methodology and stability of the LC-MS system. Raw data for the UPLC–MS/MS were obtained from Compound Discover (3.0, Thermo) based on the m/z value and the retention time of the ion signals. To ensure consistency and efficacy of the system, multiple QC samples were formulated through a combination of identical quantities of each isolated sample. The instrument's performance and repeatability were evaluated through pooled QC samples that were injected before the sample analysis until equilibrium was reached. The QC

samples were subsequently run in positive mode. The ion characteristics of the QC samples were utilized to determine the Relative Standard Deviation (RSD). Supplementary Figure S1 of the Supplementary Material displays the percentage of RSD distribution, with a significant portion of the RSD being below 30%. This indicates that the analytical method is reliable and appropriate for application to future sample analyses.

Identification of metabolites

Metabolite identification was performed at a putative level (MSI level 2) utilizing accurate mass measurements and MS/MS fragmentation data. Candidate metabolites were annotated by matching experimental spectra against the Human Metabolome Database[1], ChemSpider[2] and MassBank[3], all accessed 19 August 2024. Then manual evaluation of retention time consistency, isotope patterns, and MS/MS fragmentation spectra was done. Cross-validation across databases was achieved to enhance annotation confidence. Features detected in the ESI^+ mode were cross-checked for chromatographic and spectral consistency and combined where appropriate. Redundant ions and adducts were resolved utilizing mass accuracy criteria (<5 ppm), retention-time coherence, signal intensity, and % RSD across technical replicates to reduce duplication or erroneous assignments.

Pharmacokinetic and drug-likeness activity of differential metabolites

The properties of the ADME of significant metabolites were extrapolated through *in silico* methods, and their potential, along with their suitability as drug candidates, was evaluated. The SWISSADME platform[4] (accessed on 12 July 2025) was utilized for primary screening, which facilitated the high ranking of compounds that exhibited drug-like profiles and advantageous pharmacokinetic properties. Subsequently, further assessments were carried out with the assistance of recognized cheminformatics inclined tools for a more thorough evaluation of the pharmaceutical relevance of the metabolites. The parameters examined comprised physicochemical descriptors, which included molecular weight, number of heavy aromatic atoms, topological polar surface area (TPSA), molecular refractivity, number of hydrogen bonds, lipophilicity factors (logP), water solubility (logS), along other parameters were examined. Pharmacokinetic traits such as blood–brain barrier (BBB) permeation, gastrointestinal (GI) absorption, substrate specificity for P-glycoprotein (P-gp), inhibition potential essential key cytochrome P450 (CYP) isoenzymes (CYP1A2, CYP2C19, CYP2C9, CYP2D6, and CYP3A4), as well as skin permeation (logKp) were evaluated, and these aspects conjointly affect the metabolism of the potential and the likelihood of drug-to-drug interactions. Ultimately, the final analysis for drug-likeness was conducted using Lipinski, Ghose, Veber, Egan, Muegge, and bioavailability scores. These assessments provide a comprehensive view of the compounds' appropriateness for further progression.

Statistical analysis

In terms of anti-cancer analysis, GraphPad Prism version 8.2.0 (GraphPad Software, Inc., San Diego, CA, United States) was utilized to plot the dose-response curve and determine the IC_{50} of plant treatments.

While for metabolomics analysis, the raw data was collected and aligned utilizing Compound Discover (3.0, Thermo) according to the m/z values and the retention time of the ion signals. Ions from both ESI+ were combined and subsequently transferred into the SIMCA-P software (version 14.1) and Metaboanalyst version 6.0[5] (accessed on 12 August 2025) for multivariate analysis. Unsupervised principal component analysis (PCA) was achieved to evaluate intrinsic clusters and the structure of variance. Supervised partial least squares-discriminant analysis (PLS-DA) and orthogonal PLS-DA (OPLS-DA) were also achieved for maximizing class segregation and assessing statistically significant metabolites. Cross-validation of these models was completed, and the variance percentages clarified through orthogonal and predictive components were verified.

Statistically significant metabolites were verified and filtered by integrating the outcomes of the Variable Importance in Projection (VIP) score greater than 1.5, a p-value less than 0.05, FDR-adjusted $p < 0.05$ and a fold change (FC) greater than 2.0. The R^2 and Q^2 values can explain the quality of the fitted model. R^2 shows the variance accounted for in the model and reflects the goodness of the fit. Q^2 shows the variability in the data, reflecting the model's predictability.

Results

Anti-cancer activities

The anti-cancer activities of *A. calamus* and *L. javanica* extracts on SH-SY5Y neuroblastoma cells were assessed

1 www.hmdb.ca

2 www.chemspider.com

3 www.massbank.jp

4 http://www.swissadme.ch/index.php

5 https://www.metaboanalyst.ca

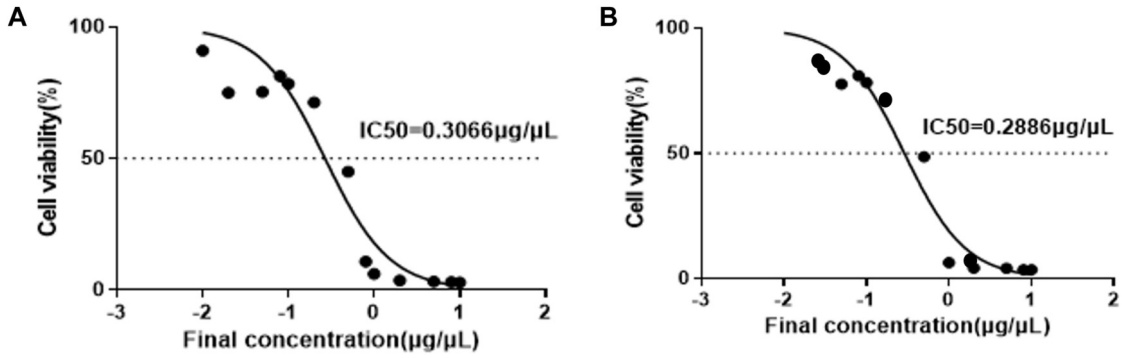

FIGURE 1
Dose-response curves for **(A)** *A. calamus* and **(B)** *L. javanica* extracts on SH-SY5Y neuroblastoma cells utilizing the CCK-8 assay.

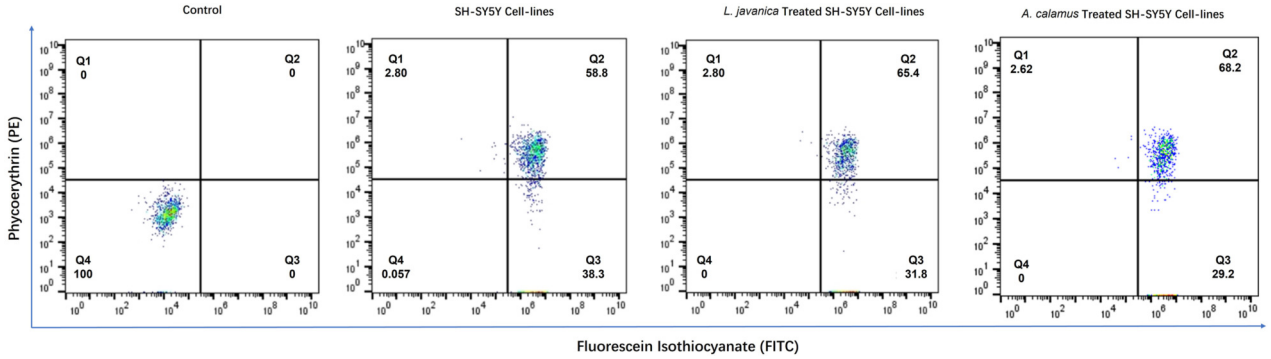

FIGURE 2
Mitochondrial membrane potential (ΔΨm) analysis of SH-SY5Y neuroblastoma cells using the JC-1 fluorescent probe and flow cytometry.

utilizing the CCK-8 assay. These plant extracts displayed a clear dose-dependent decrease in cell viability, as demonstrated by the sigmoidal dose-response curves (Figure 1). The estimated half maximal inhibitory concentration (IC_{50}) values were 0.2886 μg/μL for *A. calamus* and 0.3066 μg/μL for *L. javanica*, with 0.2976 μg/μL as an overall IC_{50} mean. However, *A. calamus* displayed slightly higher effectiveness in comparison to *L. javanica*.

Mitochondrial membrane potential analysis

Mitochondrial function in SH-SY5Y neuroblastoma cells was evaluated using flow cytometry and the JC-1 fluorescent probe to quantify variations in membrane potential (ΔΨm). As illustrated in Figure 2, in terms of untreated SH-SY5Y control cells, 58.8% of the population was within the Q2 gate, signifying cells with high ΔΨm (red fluorescence), although 38.3% of the population was situated in the Q3 gate, conforming to mitochondrial depolarization (green fluorescence). Following plant extract treatment, the proportion of the cells with high ΔΨm increased to 68.2% for *A. calamus* and 65.4% for *L. javanica*, implying increased mitochondrial polarization comparative to untreated controls.

UPLC-MS/MS base peak intensity chromatograms

The UPLC-MS/MS analysis of *A. calamus* and *L. javanica* completed in ESI+ mode produced (BPI) chromatograms, a wide profile of metabolites eluting over a specified retention time frame, as shown in Figure 3.

The chromatogram of *A. calamus* with the dominating of a particularly intense peak at ~400 s, with a highest intensity of ~1.2×10^{10}. Subsequent moderate peaks were detected at ~700, ~550, ~200, and ~50 s. Conversely, *L. javanica* offered an evenly

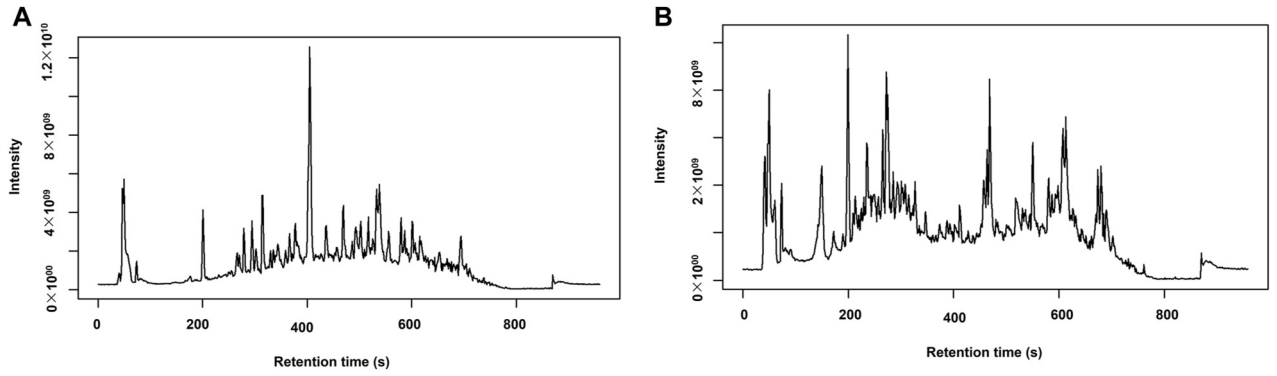

FIGURE 3
Base peak intensity (BPI) chromatograms from **(A)** *A. calamus* and **(B)** *L. javanica* in ESI+ mode.

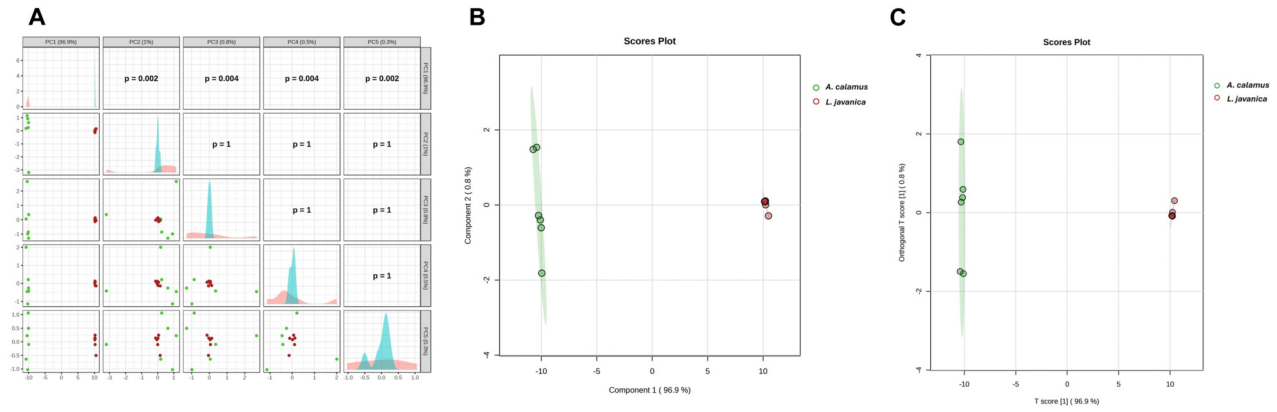

FIGURE 4
Multivariate analysis: **(A)** Principal Component Analysis (PCA) pairwise scatterplots, **(B)** Partial Least Squares Discriminant Analysis (PLS-DA) scores plot, and **(C)** Orthogonal Partial Least Squares Discriminant Analysis (OPLS-DA) scores plot of *A. calamus* (green) and *L. javanica* (red).

dispersed chromatographic profile with multiple peaks of medium to high intensity detected between 100s and 600s. The most intense peak occurred at ~220 s (~4.0 × 10^9). Additional prominent peaks were detected at ~720, ~600, ~400, and ~100 s.

Multivariate analysis of *A. calamus* and *L. javanica* data

Principal Component Analysis (PCA) score model of the associated features displays complete species segregation across PC1, with a variance of 96.9% (PC2 = 1.0%). The PCA pair-plot validates that cluster variances are concentrated on the first component and also noticeable, but smaller on higher components. The dispersals of scores vary significantly for PC2: p = 0.002, PC3: p = 0.004, PC4: p = 0.004, and PC5: p = 0.002 (Figure 4A). These results signify the possession of distinct global metabolomic fingerprints of the two species, dominated by variance expressed on PC1. The observed clustering patterns were statistically significantly validated using the PERMANOVA test, consisting of an F-value of 936.71, a p-value = 0.005, and R^2 = 0.98944.

Moreover, supervised Partial Least Squares-Discriminant Analysis (PLS-DA) generated the same qualitative pattern of PCA score model with distinct separated clusters driven by component 1 (96.9%), though component 2 represented insignificant variance of 0.8% (Figure 4B). Cross-validation metrics also validate with R^2 and Q^2 values that were close to 1.0 for all 5 tested components, which displayed consistently high performance. Moreover, the permutation test additionally validated the PLS-DA model, with a noticeable statistic positioned (p < 0.01, 0/100) that was distant outside the permutation distribution (Supplementary Figure S2).

TABLE 1 Differential metabolites distinguished from *A. calamus* and *L. javanica* in electrospray ionization ESI+ mode.

Compound name	RT (min)	Molecular Weight	*m/z*	HMDB_ID	Formula	Log^2(FC)	T-Test	FDR Log10 (p-adj)	VIP
ALKALOIDS									
5-Isothiocyanatoindane	3,015	115,17	157,1334	CSID642931	$C_6H_{13}NO$	-6,7198	4,54E-05	4,342703	1,830521
3-Indolehydracrylic acid	3,336	205,0736	206,0809	HMDB0059765	$C_{11}H_{11}NO_3$	5,338881	2,95E-05	4,52994	1,634694
Hydrocotarnine	4,956	221,1048	222,1121	HMDB0033701	$C_{12}H_{15}NO_3$	5,347002	4,08E-08	7,38938	1,6638
Mescaline	2,991	211,26	229,1543	HMDB0254474	$C_{11}H_{17}NO_3$	5,105346	4,88E-05	4,311856	1,602307
Perlolyrine	4,972	264,0895	265,0967	HMDB0030327	$C_{16}H_{12}N_2O_2$	-5,99531	0,001842	2,73468	1,680894
Prodolic acid	5,075	273,33	296,1276	HMDB0256794	$C_{16}H_{19}NO_3$	-6,27265	0,001789	2,747286	1,732869
CARBOHYDRATES									
Isopropyl β-glucoside	3,5	222,24	245,1016	HMDB0032705	$C_9H_{18}O_6$	10,83254	3,52E-05	4,453856	2,331036
Muramic acid	3,206	251,1014	252,1087	HMDB0003254	$C_9H_{17}NO_7$	8,105161	9,48E-05	4,023081	2,006866
1-O-Caffeoyl-beta-glucose	5,172	342,0944	343,1016	HMDB0302440	$C_{15}H_{18}O_9$	7,814332	1,86E-06	5,730844	1,977503
Cellulose, microcrystalline	2,156	370,35	393,136	HMDB0032197	$C_{14}H_{26}O_{11}$	6,787933	8,9E-06	5,050728	1,842234
O-Desmethyltramadol glucuronide	3,259	425,50	448,1957	HMDB0060856	$C_{21}H_{31}NO_8$	-6,19442	2,12E-05	4,673131	1,758105
Persicogenin 3'-glucoside	4,747	456,1638	479,1532	HMDB0041398	$C_{23}H_{26}O_{11}$	8,080171	1,16E-06	5,934704	2,012623
Hetastarch	4,045	736,70	759,2936	HMDB0253113	$C_{29}H_{52}O_{21}$	8,836521	2,09E-05	4,679721	2,134599
LIPIDS									
4-Methyl-2-pentenoic acid	4,046	114,14	156,1018	HMDB0031561	$C_6H_{10}O_2$	6,668955	6,85E-05	4,164162	1,833963
Undecylenic acid	4,113	184,27	226,1798	HMDB0033724	$C_{11}H_{20}O_2$	7,923542	8,84E-08	7,053706	2,029285
12-Hydroxydodecanoic acid	7,277	216,32	239,1638	HMDB0002059	$C_{12}H_{24}O_3$	-5,60027	1,14E-05	4,941239	1,679658
11-Dodecenoic acid	4,664	198,30	262,1797	HMDB0032248	$C_{12}H_{22}O_2$	6,21621	1,46E-06	5,834954	1,771416
9-Pentadecenoic acid	10,834	240,38	263,2002	HMDB0029765	$C_{15}H_{28}O_2$	-5,45158	0,000253	3,59735	1,674411
Stearidonic acid	9,676	276,40	299,1999	HMDB0006547	$C_{18}H_{28}O_2$	4,57766	1,96E-07	6,707939	1,521083
MG(18:3/0:0/0:0)	8,725	352,2605	353,2678	HMDB0011570	$C_{21}H_{36}O_4$	5,971525	2,8E-07	6,553359	1,761732
Prostaglandin A2	7,707	334,40	357,2028	HMDB0002752	$C_{20}H_{30}O_4$	7,579842	0,000121	3,916245	1,940373
Eicosanedioic acid	10,522	342,50	365,2678	HMDB0242141	$C_{20}H_{38}O_4$	6,161779	5,82E-06	5,23503	1,764398
Thromboxane B3	4,446	368,50	386,2529	HMDB0005099	$C_{20}H_{32}O_6$	-6,81951	0,000823	3,084822	1,814574
MG(5-iso PGF2VI/0:0/0:0)	6,209	400,50	423,2344	HMDB0260485	$C_{21}H_{36}O_7$	6,891431	1,09E-05	4,962081	1,86861
LysoPA(18:2/0:0)	4,868	434,50	457,2398	HMDB0007856	$C_{21}H_{39}O_7P$	6,062893	1,42E-06	5,847397	1,754746

(*Continued*)

10.3389/ebm.2026.10867

TABLE 1 Continued

Compound name	RT (min)	Molecular Weight	*m/z*	HMDB_ID	Formula	Log^2(FC)	T-Test	FDR Log10 (p-adj)	VIP
DG(20:4-2OH/0:0/2:0)	8,79	452,60	475,2682	HMDB0297002	$C_{25}H_{40}O_7$	-8,77228	1,31E-05	4,882486	2,094746
DG(2:0/PGD2/0:0)	7,165	468,60	491,2629	HMDB0296907	$C_{25}H_{40}O_8$	-5,07408	0,000151	3,820683	1,583894
DG(6 keto-PGF1alpha/2:0/0:0)	4,095	486,60	528,3155	HMDB0296912	$C_{25}H_{42}O_9$	5,338498	0,000864	3,063593	1,605199
LysoPE(22:2/0:0)	10,093	533,3475	534,3547	HMDB0011522	$C_{27}H_{52}NO_7P$	-6,18444	0,00202	2,694655	1,568301
NITROGEN COMPOUND									
1,3-Hexadien-3-amine	1,032	97,0895	98,09678	CSID67029750	$C_6H_{11}N$	6,805566	9,38E-06	5,027828	1,856891
2-Aminocyclohexanecarboxylic acid	1,229	143,0945	144,1017	CSID133327	$C_7H_{13}NO_2$	5,478209	4,02E-06	5,395528	1,656544
7-Aminomethyl-7-carbaguanine	1,725	179,0804	180,0877	HMDB0011690	$C_7H_9N_5O$	7,746392	4,59E-06	5,33773	2,019233
5-Fluoromethylornithine	4,624	164,18	187,0863	HMDB0245493	$C_6H_{13}FN_2O_2$	5,535211	8,43E-08	7,073976	1,674376
Succinyl proline	3,047	215,20	238,0682	CSID168469	$C_9H_{13}NO_5$	7,81002	9,47E-08	7,02377	1,978274
erythro-4-Hydroxyarginine	3,109	190,20	229,0704	HMDB0034326	$C_6H_{14}N_4O_3$	6,393116	3,43E-07	6,464989	1,81208
Pantothenic acid	9,416	219,23	237,1402	HMDB0000210	$C_9H_{17}NO_5$	-6,60822	0,000512	3,290701	1,785286
Phenylalanyl-Glycine	4,839	222,24	245,0917	HMDB0304788	$C_{11}H_{14}N_2O_3$	4,586087	6,19E-06	5,208442	1,522839
Glutaminylleucine	3,04	259,30	277,1906	HMDB0028801	$C_{11}H_{21}N_3O_4$	7,790423	1,82E-05	4,74028	1,971685
Glycyl-Tryptophan	3,196	261,279	279,1448	HMDB0028852	$C_{13}H_{15}N_3O_3$	-6,59597	0,001815	2,741203	1,589188
N-Acetyllactosamine	2,923	383,35	406,1337	HMDB0001542	$C_{14}H_{25}NO_{11}$	6,16663	0,000286	3,544322	1,745963
NUCLEOSIDE / NUCLEOTIDE									
2-Deoxy-ribono-1,4-lactone	5,407	132,0422	133,0495	HMDB0033958	$C_5H_8O_4$	4,608802	2,27E-05	4,644565	1,515139
2',3'-Didehydro-2',3'-dideoxycytidine	4,434	209,0811	210,0884	HMDB0245545	$C_9H_{11}N_3O_3$	-8,76604	1,28E-05	4,892618	2,092533
Keto-3-deoxy-manno-octulosonic acid	3,079	238,19	261,0601	HMDB0244292	$C_8H_{14}O_8$	6,750766	4,57E-06	5,340459	1,856524
5-(Hydroxymethyl)cytidine	2,821	273,0955	274,1027	CSID32720391	$C_{10}H_{15}N_3O_6$	4,788076	2,22E-06	5,653688	1,616127
2',3'-Dideoxyadenosine	6,718	235,24	277,1405	HMDB0245544	$C_{10}H_{13}N_5O_2$	-6,84114	4,18E-05	4,379233	1,84559
5-Methyldeoxycytidine	2,036	241,24	283,1396	HMDB0002224	$C_{10}H_{15}N_3O_4$	-8,43195	0,00119	2,924626	1,881698
3'-C-Ethynylcytidine	3,174	267,24	309,1174	HMDB0252093	$C_{11}H_{13}N_3O_5$	8,752045	3,19E-08	7,496043	2,107001
2'-Deoxy-5-formylcytidine	1,99	255,23	319,0993	CSID10291642	$C_{10}H_{13}N_3O_5$	5,632298	2,15E-06	5,666959	1,744307
Dimp	4,25	332,0524	333,0597	HMDB0006555	$C_{10}H_{13}N_4O_7P$	8,036495	2,38E-07	6,623169	2,006318
2-Methylguanosine	4,679	297,27	339,1407	HMDB0005862	$C_{11}H_{15}N_5O_5$	-5,73448	0,000162	3,789346	1,681938

(*Continued*)

10.3389/ebm.2026.10867

TABLE 1 Continued

Compound name	RT (min)	Molecular Weight	*m/z*	HMDB_ID	Formula	Log^2(FC)	T-Test	FDR Log10 (p-adj)	VIP
OTHER									
2,4-Pentadienal	10,135	82,04236	83,04964	HMDB0031597	C_5H_6O	7,510876	1,41E-06	5,850963	1,943115
5-Methylcytosine	6,097	125,0603	126,0676	HMDB0002894	$C_5H_7N_3O$	-8,4848	4,81E-06	5,317795	2,059602
xi-4-Hydroxy-4-methyl-2-cyclohexen-1-one	3,795	126,0681	127,0754	HMDB0033629	$C_7H_{10}O_2$	8,258472	6,02E-06	5,22045	2,034825
gamma-Butyrolactone	3,78	86,09	128,0706	HMDB0000549	$C_4H_6O_2$	7,403507	6,82E-06	5,166232	1,925084
Indol-2-one	3,251	131,0371	132,0444	HMDB0253466	C_8H_5NO	5,862663	3,16E-07	6,500593	1,718906
Methyl 2-thiofuroate	0,897	142,0115	143,0188	HMDB0037762	$C_6H_6O_2S$	4,48824	1,48E-05	4,829513	1,511626
Norcamphoric acid	3,195	158,15	200,0915	CSID207959	$C_7H_{10}O_4$	5,611922	7,34E-06	5,134455	1,720562
4-Guanidino-1-butanol	0,787	131,18	173,1396	CSID4476579	$C_5H_{13}N_3O$	-5,88882	0,001006	2,997208	1,515761
1-Oxo-1H-2-benzopyran-3-carboxaldehyde	4,626	174,0315	175,0388	HMDB0030577	$C_{10}H_6O_3$	6,426311	1,56E-05	4,807221	1,825317
3-Hydroxysuberic acid	2,866	190,19	232,1191	HMDB0000325	$C_8H_{14}O_5$	4,813224	4,4E-06	5,356159	1,568506
6-(2-Hydroxyethoxy)-6-oxohexanoic acid	3,717	190,19	213,0755	HMDB0061681	$C_8H_{14}O_5$	4,69247	4,65E-06	5,332964	1,552665
N-Lactoylphenylalanine	4,391	215,1177	238,1069	HMDB0062175	$C_{12}H_{15}NO_4$	5,606803	5,75E-07	6,240409	1,704328
2-(2-Furylmethyl)-1-indanol	3,905	214,26	237,0907	CSID40514807	$C_{14}H_{14}O_2$	-5,2121	0,000218	3,660803	1,591246
Piperdial	6,936	250,1565	251,1638	HMDB0035798	$C_{15}H_{22}O_3$	-5,12368	4,52E-06	5,345311	1,600008
1-(Ribofuranosyl)indoline	2,641	251,1153	252,1226	CSID67029342	$C_{13}H_{17}NO_4$	4,946661	1,05E-05	4,977423	1,570688
2-Hydroxyacorenone	9,271	236,35	259,1664	HMDB0030916	$C_{15}H_{24}O_2$	-7,68915	1,73E-06	5,761784	1,961428
Risbitin	5,609	222,32	264,1954	HMDB0302980	$C_{14}H_{22}O_2$	-5,92921	0,001049	2,979129	1,703258
Linamarin	1,312	247,24	270,0944	HMDB0033699	$C_{10}H_{17}NO_6$	-6,29487	0,000877	3,056864	1,759135
1-Hydroxyacorenone	7,673	250,33	273,1456	HMDB0030917	$C_{15}H_{22}O_3$	-7,10849	1,82E-06	5,739609	1,887368
4-Hydroxycyclohexylcarboxylic acid	4,619	144,17	289,1637	HMDB0001988	$C_7H_{12}O_3$	6,014314	5,86E-06	5,232144	1,73907
Pollenin A	4,254	302,042	303,0493	HMDB0303704	$C_{15}H_{10}O_7$	8,76912	2,16E-07	6,664657	2,126655
9,10-DiHODE	4,767	312,40	330,2632	HMDB0010221	$C_{18}H_{32}O_4$	-4,97006	0,000693	3,159427	1,553509
6β–Hydroxymethandienone	10,138	316,40	339,1922	HMDB0005832	$C_{20}H_{28}O_3$	10,73503	2,66E-06	5,575855	2,317918
Bisoprolol	5,313	325,40	348,2162	HMDB0014750	$C_{18}H_{31}NO_4$	5,110144	2,27E-05	4,643337	1,607036
6'-Hydroxyenterolactone	4,893	314,30	356,1482	HMDB0041697	$C_{18}H_{18}O_5$	6,599311	0,00027	3,568419	1,804397
Caryoptosidic acid	2,971	392,35	415,1204	HMDB0034249	$C_{16}H_{24}O_{11}$	6,037738	0,000224	3,649573	1,731817
Tyromycic acid	12,521	452,3278	453,3351	HMDB0035888	$C_{30}H_{44}O_3$	-5,71222	4,22E-05	4,374993	1,690313

(*Continued*)

10.3389/ebm.2026.10867

TABLE 1 Continued

Compound name	RT (min)	Molecular Weight	*m/z*	HMDB_ID	Formula	Log^2(FC)	T-Test	FDR Log10 (p-adj)	VIP
Fluocinolone	2,966	412,4	454,2062	HMDB0252347	$C_{21}H_{26}F_2O_6$	-5,03287	0,000493	3,307314	1,561579
Persiconin	4,285	478,1466	479,1539	HMDB0037482	$C_{23}H_{26}O_{11}$	8,487737	1,03E-06	5,987367	2,064423
Phaseolus epsilon	3,657	526,50	544,2378	HMDB0035039	$C_{25}H_{34}O_{12}$	7,87868	7,04E-05	4,152464	1,979816
19-Nor-5-androstenediol	9,685	276,40	553,4239	HMDB0004590	$C_{18}H_{28}O_2$	7,24471	8,58E-06	5,066603	1,926738
7-Dehydrologanin tetraacetate	3,488	556,1755	557,1828	CSID391585	$C_{25}H_{32}O_{14}$	-6,16628	0,003738	2,427367	1,709022
Procyanidin	3,823	578,1412	579,1484	HMDB0013690	$C_{30}H_{26}O_{12}$	-7,188	0,000208	3,681349	1,883821
Desglucocheirotoxol	13,088	552,70	591,2582	HMDB0033828	$C_{29}H_{44}O_{10}$	5,752651	2,39E-05	4,621974	1,696989
Neolicuroside	3,869	550,50	592,201	HMDB0040728	$C_{26}H_{30}O_{13}$	8,370981	5,7E-06	5,243925	2,048135
Marmesin rutinoside	2,724	554,50	596,2325	HMDB0041413	$C_{26}H_{34}O_{13}$	-6,94662	0,0022	2,657484	1,81168
Hesperidin methylchalcone	4,557	624,2032	625,2106	HMDB0253112	$C_{29}H_{36}O_{15}$	9,090381	1,04E-08	7,982463	2,139523
Glucoliquiritin apioside	3,01	712,60	730,2684	HMDB0041149	$C_{32}H_{40}O_{18}$	-6,08309	0,00112	2,950734	1,673043
Leonoside A	4,557	770,70	788,2936	HMDB0040342	$C_{35}H_{46}O_{19}$	9,611505	1,25E-05	4,904459	2,19735
PHENOLIC									
Coumarin	2,503	146,0365	147,0438	HMDB0001218	$C_9H_6O_2$	5,452435	0,000132	3,879057	1,64696
3 Hydroxycoumarin	4,771	162,0314	163,0387	HMDB0002149	$C_9H_6O_3$	4,910609	2,63E-07	6,580547	1,573768
4,8-Dimethyl-7-hydroxycoumarin	3,343	190,19	208,0965	CSID4512230	$C_{11}H_{10}O_3$	5,339346	1,67E-05	4,77794	1,635275
Vanillactic acid	1,727	212,0682	213,0755	HMDB0000913	$C_{10}H_{12}O_5$	7,713922	6,68E-07	6,175003	1,979313
Apigenin	5,177	270,0523	271,0596	HMDB0002124	$C_{15}H_{10}O_5$	5,845909	7,92E-05	4,101263	1,718134
Kaempferol	4,724	286,047	287,0542	HMDB0005801	$C_{15}H_{10}O_6$	7,038508	1,48E-06	5,830917	1,898751
3-Feruloyl-1,5-quinolactone	4,631	350,30	373,091	HMDB0029289	$C_{17}H_{18}O_8$	7,663669	2,15E-05	4,668116	1,956575
2-trans-O-Feruloylglucaric acid	3,606	386,0841	387,0913	HMDB0302546	$C_{16}H_{18}O_{11}$	9,917521	9,38E-06	5,027846	2,226979
Glucosyloxyanthraquinone	3,844	386,40	409,0911	CSID389045	$C_{20}H_{18}O_8$	-5,23257	0,000103	3,987626	1,611837
Eriodictin	4,559	434,1204	435,1277	HMDB0037480	$C_{21}H_{22}O_{10}$	8,417998	1,65E-10	9,781596	2,058779
Catechin 7-glucoside	3,177	452,131	453,1383	HMDB0037949	$C_{21}H_{24}O_{11}$	-5,3561	0,003285	2,483526	1,591291
Quercetin 3-O-glucuronide	4,241	478,0739	479,0812	HMDB0029212	$C_{21}H_{18}O_{13}$	9,420172	6,67E-08	7,175578	2,186479
Sesaminol glucoside	7,259	532,50	555,1482	HMDB0041209	$C_{26}H_{28}O_{12}$	4,976722	7,32E-05	4,135256	1,570614
Apigenin 7-O-diglucuronide	4,027	622,1149	623,1222	HMDB0301685	$C_{27}H_{26}O_{17}$	9,063099	3,86E-07	6,413527	2,131068
Tetramethylquercetin 3-rutinoside	4,052	666,60	708,2469	HMDB0039337	$C_{31}H_{38}O_{16}$	11,67918	1,57E-06	5,804899	2,418616

(*Continued*)

10.3389/ebm.2026.10867

TABLE 1 Continued

Compound name	RT (min)	Molecular Weight	*m/z*	HMDB_ID	Formula	Log^2(FC)	T-Test	FDR Log10 (p-adj)	VIP
POLYKETIDES									
1(2H)-Pentalenone	2,502	118,042	119,0493	CSID66739022	C_8H_6O	4,673748	0,000182	3,739442	1,516804
Phthalide	2,503	134,13	157,0282	HMDB0032469	$C_8H_6O_2$	8,291181	0,000232	3,634062	2,029866
Aflatoxin G2	6,708	330,0731	331,0804	HMDB0030475	$C_{17}H_{14}O_7$	7,294113	0,000298	3,526371	1,900981
TERPENOIDS									
Shinanolone	4,667	192,075	193,0823	HMDB0030580	$C_{11}H_{12}O_3$	-5,65953	0,005135	2,289432	1,589457
4,7-Megastigmadien-9-ol	8,59	194,1668	195,1741	HMDB0038731	$C_{13}H_{22}O$	-5,78981	3,46E-05	4,460445	1,700406
Vomifoliol	3,517	224,1409	225,1482	HMDB0303570	$C_{13}H_{20}O_3$	6,685312	3,63E-06	5,439498	1,850491
7-Epi-12-hydroxyjasmonic acid	3,942	226,12	227,1273	HMDB0303749	$C_{12}H_{18}O_4$	9,757035	2,83E-08	7,548945	2,218914
8-Hydroxygeraniol 8-O-glucoside	4,457	332.39	374,2165	HMDB0035025	$C_{16}H_{28}O_7$	5,392225	0,000565	3,248129	1,621572
3beta-Hydroxy-5-cholestenal	9,848	400,60	423,3249	HMDB0060131	$C_{27}H_{44}O_2$	-5,19836	1,33E-05	4,874901	1,62304
7a,12a-Dihydroxy-cholestene-3-one	10,46	416,60	439,3199	HMDB0002197	$C_{27}H_{44}O_3$	-7,53264	7,79E-06	5,108677	1,956674
Limonoate a-ring-lactone	6,644	488,2015	489,2088	HMDB0302537	$C_{26}H_{32}O_9$	-5,00973	0,001182	2,927482	1,561349
Cucumerin A	2,79	552,50	575,1571	HMDB0301967	$C_{29}H_{28}O_{11}$	6,765172	0,000685	3,164562	1,819729
Cholic acid glucuronide	12,017	584,70	623,2843	HMDB0002577	$C_{30}H_{48}O_{11}$	4,8136	9,02E-06	5,04476	1,549668
Linalool (8-hydroxydihydro-)	4,627	650,70	692,2884	HMDB0304700	$C_{32}H_{42}O_{14}$	6,441235	4,01E-05	4,396548	1,794936

Key: Highlighted top ten differential metabolites distinguished between *A. calamus* and *L. javanica*.

10.3389/ebm.2026.10867

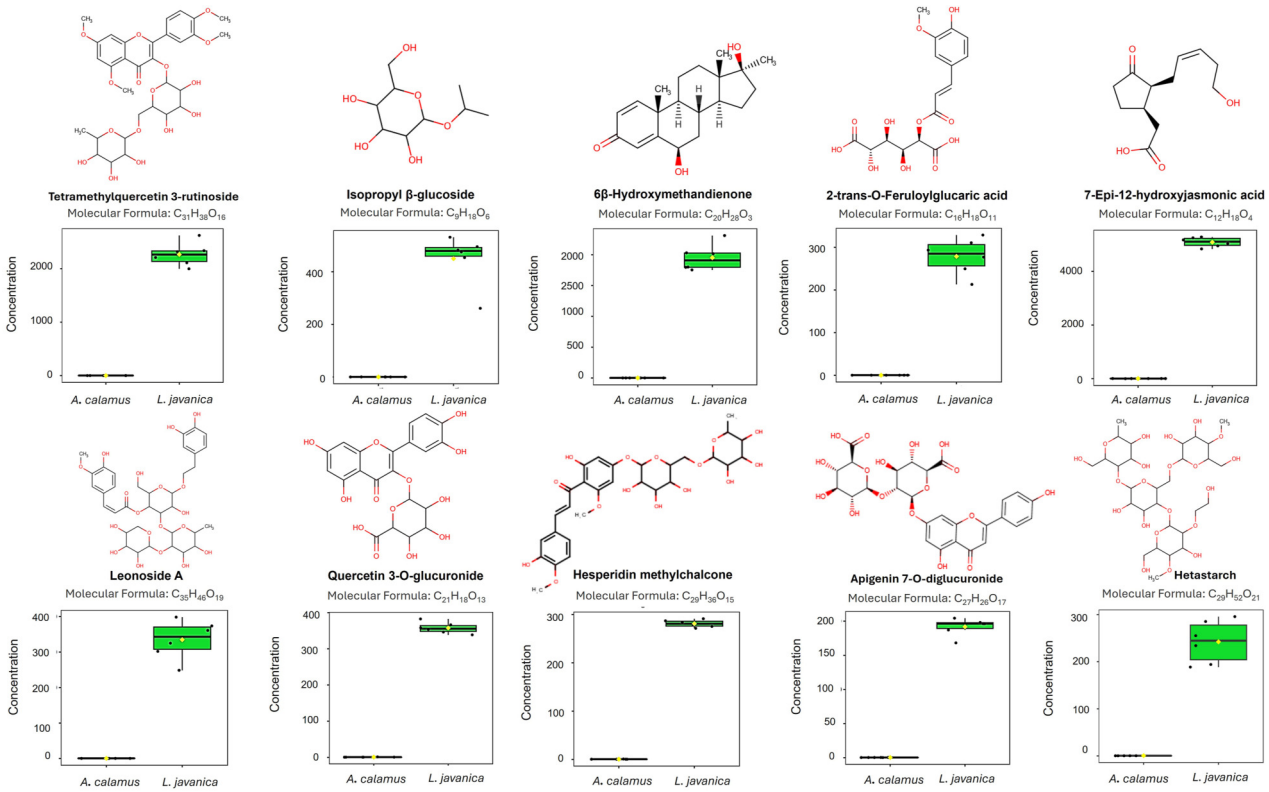

FIGURE 5
Differential metabolites distinguished between *A. calamus* and *L. javanica*. Molecular formulas, chemical structures, and boxplots of the top ten compounds (VIP >1.5, FC >2.0, $p < 0.05$, FDR-adjusted $p < 0.05$) are shown, with abundances in *A. calamus* and *L. javanica*.

Orthogonal PLS-DA (OPLS-DA) model additionally displays variation into a single predictive component (T score [1] = 96.9%) that segregates the plant species and an orthogonal component (Orthogonal T score [1] = 0.8%) representing within the class structure (Figure 4C). The model was further validated by cross-validation, where the model generated high explanatory and predictive performance, with $R^2Y = 1.0$, $R^2X = 0.969$, and $Q^2 = 0.999$. The related p-values for the predictive component (p1) were R^2X: 0.969; R^2Y: 1.0; Q^2: 0.999, whereas for the orthogonal component (o1) were R^2X: 0.00813, R^2Y: 0.00031, and Q^2: 7.04×10^{-5}, underscoring the model's explanatory and predictive capability. Further validation of the model was done using a permutation test, with Q^2 and R^2Y values of 0.969 and 0.979, respectively (Supplementary Figure S2).

Univariate analysis of *A. calamus* and *L. javanica* data

Univariate analysis recognized the top ten metabolites with VIP >2.0, FC >2.0, $p < 0.05$ and FDR-adjusted $p < 0.05$ that significantly differentiated the clusters of *A. calamus* and *L. javanica* (Table 1). Figure 5 depicts major significant metabolites comprising Tetramethylquercetin 3-rutinoside, Isopropyl β-glucoside, and 6β-Hydroxymethandienone, altogether presenting an extreme fold of enrichment. Further significant metabolites comprised of 2-trans-O-Feruloylglucaric acid, 7-Epi-12-hydroxyjasmonic acid, and Leonoside A. Flavonoid derivatives, for instance Quercetin 3-O-glucuronide, Hesperidin methylchalcone, and Apigenin 7-O-diglucuronide were also significantly differentiated. Additionally, Hetastarch also provided a contribution to the metabolic variance. Together, these compounds underscore jasmonates, flavonoid glycosides, and phenolic derivatives as crucial, statistically significant metabolites, supporting the distinct chemical divergence amongst the two plant species. These compounds show higher abundances constantly in *L. javanica* (Figure 5). A detailed chemical profiling of each compound is represented in the Supplementary Table S1.

Pharmacokinetic and drug-likeness activity of differential metabolites

The assessment of the ten most significant metabolites from *A. calamus* and *L. javanica* was conducted through the SWISSADME platform to acquire the ADME profiles of each

significant metabolite. This yields essential insights into their potential efficacy as neuroactive inhibitors targeting SH-SY5Y neuroblastoma cells (Table 2).

Physicochemical properties

There was a considerable amount of variability in molecular weight, polarity, and solubility of the ten-highest ranked metabolites, which was determined using the SWISSADME. Smaller molecules such as 7-epi-12-hydroxyjasmonic acid (MW 226.27 g/mol) and isopropyl β-glucoside (MW 222.24 g/mol) had a low topological polar surface area (TPSA <60 $Å^2$) and the absence of hydrogen bond donors, indicating a pronounced potential for passive permeability across biological membranes, and these molecules also met the physicochemical criteria for drug-like entities. In contrast, more complex glycosylated flavonoids, such as apigenin 7-O-diglucuronide (MW 622.49 g/mol) and Leonoside A (MW 770.73 g/mol), exhibited slightly elevated TPSA (>250 $Å^2$) and standout characteristics such as multiple hydrogen bond donors/acceptors, which are conventionally linked to restricted oral bioavailability.

The indices (consensus Log Po/w) for lipophilicity varied from −5.27 for hetastarch to 4.45 for 6β-hydroxymethandienone. This specifically emphasizes the solubility-permeability trade-offs across the metabolite library. Remarkably, 6β-hydroxymethandienone displayed favorable lipophilicity alongside an acceptable molecular weight, implying a significant potential for permeability; conversely, polar glucuronides (e.g., quercetin 3-O-glucuronide, consensus Log Po/w −0.47) are likely impeded in their capacity for cellular penetration.

Water solubility

Predictions regarding water solubility indicated that hetastarch is highly soluble (>2.0 × 10^4 mg/mL), while 6β-hydroxymethandienone displayed suboptimal solubility (4.32 × 10^{-3} mg/mL). Intermediate solubility profiles were noted for flavonoid derivatives, such as hesperidin methylchalcone and tetramethylquercetin 3-rutinoside. These findings suggest that formulation strategies may be necessary for highly lipophilic compounds exhibiting poor intrinsic solubility.

Pharmacokinetics

Predictions regarding gastrointestinal (GI) absorption depicted that 6β-hydroxymethandienone, isopropyl β-glucoside, and 7-epi-12-hydroxyjasmonic acid demonstrate high absorption potential, whereas the majority of glycosylated flavonoids exhibited low absorption due to their extensive polar surface areas. Blood-brain barrier (BBB) permeability was anticipated for the smaller hydrophobic compounds, particularly isopropyl β-glucoside, 6β-hydroxymethandienone, and 7-epi-12-hydroxyjasmonic acid, implying a potential for central nervous system (CNS) activity against SH-SY5Y neuroblastoma cells. Significantly, numerous compounds, including hesperidin methylchalcone and apigenin diglucuronide, were identified as substrates for P-glycoprotein (P-gp), suggesting a vulnerability to efflux and diminished intracellular accumulation.

Skin permeation (Log Kp) values were more favorable for lipophilic scaffolds (e.g., −4.33 cm/s for 6β-hydroxymethandienone) in comparison to highly polar compounds (−16.26 cm/s for hetastarch). The analysis of Cytochrome P450 (CYP) inhibition identified 6β-hydroxymethandienone as a multi-isoform inhibitor (CYP2C19, CYP2C9, CYP2D6, CYP3A4), indicating potential drug-drug interaction liabilities, whereas the majority of glycosides exhibited no alerts for CYP inhibition.

Drug-likeness

Filters for Drug-likeness indicated that only isopropyl β-glucoside, 6β-hydroxymethandienone, and 7-epi-12-hydroxyjasmonic acid fully conformed to Lipinski's rule of five, as well as Veber, Egan, and Muegge criteria, while the majority of glycosides surpassed thresholds for hydrogen bonding, molecular weight, and TPSA. Bioavailability scores corroborated these findings, revealing favorable values of 0.55 for the smaller drug-like molecules in contrast to ≤0.17 for the larger glycosides. These outcomes underscore isopropyl β-glucoside and 6β-hydroxymethandienone as promising candidates for oral bioavailability.

Medicinal chemistry filters

The identification of Brenk alerts, as well as PAINS (Pan-Assay Interference Compounds), has highlighted various flavonoid derivatives (such as hesperidin methylchalcone, Leonoside A, and quercetin 3-O-glucuronide) that exhibit Michael acceptor motifs or catechol, thereby indicating the likelihood of assay interferences. The synthetic accessibility scores exhibited a range from 2.31 (7-epi-12-hydroxyjasmonic acid, which is readily synthesizable) to 8.06 (hetastarch, which is characterized by high complexity), reflecting considerations of feasibility for prospective lead optimization endeavors. Lead-likeness was attained solely for 6β-hydroxymethandienone, while the remaining metabolites were hindered by excessive molecular dimensions or flexibility.

Therefore, the ADME profiling has prioritized three metabolites, namely isopropyl β-glucoside, 6β-hydroxymethandienone, and 7-epi-12-hydroxyjasmonic acid, which emerge as the most promising lead-like candidates for targeting of SH-SY5Y neuroblastoma cells. Larger polar flavonoid glycosides, despite their bioactivity, may necessitate structural simplification or the implementation of advanced delivery systems to mitigate challenges related to poor absorption and permeability. Their favourable oral bioavailability, blood-brain barrier permeability, and adherence to drug-likeness criteria substantiate their potential for subsequent preclinical validation.

10.3389/ebm.2026.10867

TABLE 2 Physicochemical, pharmacokinetic, drug-likeness, and medicinal chemistry properties of the selected differential bioactive secondary metabolites.

Parameters	Isopropyl β-glucoside	Hetastarch	6β--hydroxymethandienone	Hesperidin methylchalcone	Leonoside A	2-trans-O-Feruloylglucaric acid	Quercetin 3-O-glucuronide	Apigenin 7-O-diglucuronide	Tetramethylquercetin 3-rutinoside	7-Epi-12-hydroxyjasmonic acid
Physicochemical Properties										
Formula	C9H18O6	C29H52O21	C20H28O3	C29H36O15	C35H46O19	C16H18O11	C21H18O13	C27H26O17	C31H38O16	C12H18O4
Molecular weight	222.24 g/mol	736.71 g/mol	316.43 g/mol	624.59 g/mol	770.73 g/mol	386.31 g/mol	478.36 g/mol	622.49 g/mol	666.62 g/mol	226.27 g/mol
No. heavy atoms	15	50	23	44	54	27	34	44	47	16
No. arom. heavy atoms	0	0	0	12	12	10	16	16	12	0
Fraction Csp3	1.00	1.00	0.60	0.48	0.57	0.44	0.24	0.37	0.48	0.50
No. of rotatable bonds	0	15	6	11	13	4	4	7	13	9
No. H-bond acceptors	6	21	3	15	19	11	13	17	16	4
No. H-bond donors	0	11	0	9	11	6	8	9	8	0
Molar Refractivity	49.89	156.69	93.83	148.42	179.64	87.17	110.77	139.71	158.16	61.42
TPSA	55.38 Å²	314.83 Å²	43.37 Å²	245.29 Å²	304.21 Å²	179.28 Å²	227.58 Å²	283.34 Å²	251.36 Å²	52.60 Å²
Lipophilicity										
Log Po/w (iLOGP)	3.13	2.21	4.00	2.15	2.28	0.90	1.13	0.28	3.47	3.17
Log Po/w (XLOGP3)	1.84	−7.70	5.49	−0.50	−1.60	−0.99	0.61	−0.24	0.07	2.22
Log Po/w (WLOGP)	2.05	−7.35	4.39	−1.12	−2.27	−1.61	−0.45	−1.94	−0.55	2.01
Log Po/w (MLOGP)	1.50	−7.42	3.48	−2.37	−3.75	−2.23	−2.60	−3.68	−1.99	1.94
Log Po/w (SILICOS-IT)	1.09	−6.09	4.87	−1.14	−2.61	−1.13	−1.04	−2.66	−0.61	2.53
Consensus Log Po/w	1.92	−5.27	4.45	−0.60	−1.59	−1.01	−0.47	−1.65	0.08	2.37
Water solubility										
Log S (ESOL)	−2.38	1.43	−4.86	−2.87	−2.92	−1.62	−3.27	−3.36	−3.35	−2.05
Solubility	9.33e-01 mg/mL; 4.20e-03 mol/L	2.00e+04 mg/mL; 2.71e+01 mol/L	4.32e-03 mg/mL; 1.37e-05 mol/L	8.36e-01 mg/mL; 1.34e-03 mol/L	9.33e-01 mg/mL; 1.21e-03 mol/L	9.24e+00 mg/mL; 2.39e-02 mol/L	2.54e-01 mg/mL; 5.32e-04 mol/L	2.75e-01 mg/mL; 4.41e-04 mol/L	2.99e-01 mg/mL; 4.49e-04 mol/L	2.03e+00 mg/mL; 8.96e-03 mol/L
Class	Soluble	Highly soluble	Moderately soluble	Soluble	Soluble	Very soluble	Soluble	Soluble	Soluble	Soluble

(*Continued*)

TABLE 2 Continued

Parameters	Isopropyl β-glucoside	Hetastarch	6β--hydroxymethandienone	Hesperidin methylchalcone	Leonoside A	2-trans-O-Feruloylglucaric acid	Quercetin 3-O-glucuronide	Apigenin 7-O-diglucuronide	Tetramethylquercetin 3-rutinoside	7-Epi-12-hydroxyjasmonic acid
Log S (Ali)	−2.62	1.83	−6.16	−4.18	−4.28	−2.29	−4.96	−5.25	−4.90	−2.96
Solubility	5.29e-01 mg/mL; 2.38e-03 mol/L	4.95e+04 mg/mL; 6.72e+01 mol/L	2.19e-04 mg/mL; 6.94e-07 mol/L	4.09e-02 mg/mL; 6.55e-05 mol/L	4.05e-02 mg/mL; 5.26e-05 mol/L	1.99e+00 mg/mL; 5.14e-03 mol/L	5.20e-03 mg/mL; 1.09e-05 mol/L	3.48e-03 mg/mL; 5.59e-06 mol/L	8.35e-03 mg/mL; 1.25e-05 mol/L	2.48e-01 mg/mL; 1.10e-03 mol/L
Class	Soluble	Highly soluble	Poorly soluble	Moderately soluble	Moderately soluble	Soluble	Moderately soluble	Moderately soluble	Moderately soluble	Soluble
Log S (SILICOS-IT)	−1.45	5.00	−3.83	−0.22	1.04	−0.34	−1.04	0.05	−0.81	−2.55
Solubility	7.89e+00 mg/mL; 3.55e-02 mol/L	7.45e+07 mg/mL; 1.01e+05 mol/L	4.65e-02 mg/mL; 1.47e-04 mol/L	3.77e+02 mg/mL; 6.04e-01 mol/L	8.55e+03 mg/mL; 1.11e+01 mol/L	1.75e+02 mg/mL; 4.52e-01 mol/L	4.36e+01 mg/mL; 9.12e-02 mol/L	6.95e+02 mg/mL; 1.12e+00 mol/L	1.03e+02 mg/mL; 1.55e-01 mol/L	6.35e-01 mg/mL; 2.81e-03 mol/L
Class	Soluble	Soluble	Soluble	Soluble	Soluble	Soluble	Soluble	Soluble	Soluble	Soluble
Pharmacokinetics										
GI absorption	High	Low	High	Low	Low	Low	Low	Low	Low	High
BBB permeant	Yes	No	Yes	No	No	No	No	No	No	Yes
P-gp substrate	No	Yes	No	Yes	No	No	Yes	Yes	Yes	No
CYP1A2 inhibitor	No	No	No	No	No	No	No	No	No	No
CYP2C19 inhibitor	No	No	Yes	No	No	No	No	No	No	No
CYP2C9 inhibitor	Yes	No	Yes	No	No	No	No	No	No	No
CYP2D6 inhibitor	No	No	Yes	No	No	No	No	No	No	No
CYP3A4 inhibitor	No	No	Yes	No	No	No	No	No	No	No
Log Kp (skin permeation)	−6.35 cm/s	−16.26 cm/s	−4.33 cm/s	−10.46 cm/s	−12.14 cm/s	−9.36 cm/s	−8.78 cm/s	−10.27 cm/s	−10.32 cm/s	−6.10 cm/s
Drug likeness										
Lipinski	Yes; 0 violation	No; 3 violations: MW >500, NorO >10, NHorOH >5	Yes; 0 violation	No; 3 violations: MW >500, NorO >10, NHorOH >5	No; 3 violations: MW >500, NorO >10, NHorOH >5	No; 2 violations: NorO >10, NHorOH >5	No; 2 violations: NorO >10, NHorOH >5	No; 3 violations: MW >500, NorO >10, NHorOH >5	No; 3 violations: MW >500, NorO >10, NHorOH >5	Yes; 0 violation
Ghose	Yes	No; 4 violations: MW >480, WLOGP <−0.4, MR >130, #atoms >70	Yes	No; 4 violations: MW >480, WLOGP <−0.4, MR >130, #atoms >70	No; 4 violations: MW >480, WLOGP <−0.4, MR >130, #atoms >70	No; 1 violation: WLOGP <−0.4	No; 1 violation: WLOGP<−0.4	No; 3 violations: MW >480, WLOGP<−0.4, MR >130	No; 4 violations: MW >480, WLOGP <−0.4, MR >130, #atoms >70	Yes
Veber	Yes	No; 2 violations: Rotors >10, TPSA >140	Yes	No; 2 violations: Rotors >10, TPSA >140	No; 2 violations: Rotors >10, TPSA >140	No; 1 violation: TPSA >140	No; 1 violation: TPSA >140	No; 1 violation: TPSA >140	No; 2 violations: Rotors >10, TPSA >140	Yes

(*Continued*)

10.3389/ebm.2026.10867

TABLE 2 Continued

Parameters	Isopropyl β-glucoside	Hetastarch	6β--hydroxymethandienone	Hesperidin methylchalcone	Leonoside A	2-trans-O-Feruloylglucaric acid	Quercetin 3-O-glucuronide	Apigenin 7-O-diglucuronide	Tetramethylquercetin 3-rutinoside	7-Epi-12-hydroxyjasmonic acid
Egan	Yes	No; 1 violation: TPSA >131.6	Yes	No; 1 violation: TPSA >131.6	No; 1 violation: TPSA >131.6	No; 1 violation: TPSA >131.6	No; 1 violation: TPSA >131.6	No; 1 violation: TPSA >131.6	No; 1 violation: TPSA >131.6	Yes
Muegge	Yes	No; 5 violations: MW >600, XLOGP3 <−2, TPSA >150, H-acc >10, H-don >5	No; 1 violation: XLOGP3 >5	No; 4 violations: MW >600, TPSA >150, H-acc >10, H-don >5	No; 4 violations: MW >600, TPSA >150, H-acc >10, H-don >5	No; 3 violations: TPSA >150, H-acc >10, H-don >5	No; 3 violations: TPSA >150, H-acc >10, H-don >5	No; 4 violations: MW >600, TPSA >150, H-acc >10, H-don >5	No; 4 violations: MW >600, TPSA >150, H-acc >10, H-don >5	Yes
Bioavailability score	0.55	0.17	0.55	0.17	0.17	0.17	0.11	0.11	0.17	0.55
Medicinal Chemistry										
PAINS	0 alert	0 alert	0 alert	1 alert: catechol_A	1 alert: catechol_A	0 alert	1 alert: catechol_A	0 alert	1 alert: catechol_A	0 alert
Brenk	1 alert: peroxide	0 alert	1 alert: isolated_alkene	2 alerts: catechol, michael_acceptor_1	2 alerts: catechol, michael_acceptor_1	1 alert: cumarine	1 alert: catechol	0 alert	3 alerts: catechol, michael_acceptor_1, more_than_2_esters	2 alerts: mchael_acceptor_1, more_than_2_esters
Leadlikeness	No; 1 violation: MW 250	No; 2 violations: MW >350, Rotors >7	No; 1 violation: XLOGP3 >3.5	No; 2 violations: MW >350, Rotors >7	No; 2 violations: MW >350, Rotors >7	No; 1 violation: MW >350	No; 1 violation: MW >350	No; 1 violation: MW >350	No; 2 violations: MW >350, Rotors >7	No; 2 violations: MW < 250, Rotors >7
Synthetic accessibility	4.34	8.06	4.72	6.37	7.45	5.05	5.26	6.26	6.57	2.31

10.3389/ebm.2026.10867

Discussion

This study validates that extracts of *L. javanica* and *A. calamus* alter mitochondrial functional status and exert dose-dependent cytotoxic effects in SH-SY5Y neuroblastoma cells. The observed shifting toward increased mitochondrial membrane polarization, as evaluated by JC-1 staining, implies preservation or enrichment of mitochondrial reliability at levels of the tested exposure, rather than clear mitochondrial depolarization. Such effects are consistent with complex phytochemical concoctions in which mitochondrial responses might vary depending on exposure duration, concentration, and cellular context [14, 52].

Untargeted metabolomics analysis facilitated the chemical delineation of the phenotypic expressions of substances. With multivariate statistics verifying the distinct chemical differences between the two species, the metabolomic profiling identified a wide range of bioactive substances, including alkaloids, phenolics, flavonoid glycosides, and jasmonates. Separated and distinct groupings were exhibited by *L. javanica* and *A. calamus* in PCA, PLS-DA and OPLS-DA, with cross-validation by OPLS-DA and permutation analyses corroborating the non-random nature of the segregation of classes [53]. Given the propensity for supervised models to exhibit overfitting traits, the interpretation of data of the nearly perfect R^2/Q^2 values with circumspection, anchoring conclusions within the framework of unsupervised PCA delineation and independent univariate filters (VIP, fold-change, *p* values), which is indicative of optimal methodological procedures [54]. The principal discriminative compounds identified were isopropyl β-glucoside, 6β-hydroxymethandienone, 7-epi-12-hydroxyjasmonic acid, 2-trans-O-feruloylglucaric acid, and flavonoid glycosides (e.g., conjugates of quercetin and apigenin) [55]. The identification of a jasmonate (7-epi-12-hydroxyjasmonic acid) is of significant mechanistic relevance; most jasmonates and their derivatives possess the capability to induce cancer cell apoptosis through the disassociation of hexokinase II from the mitochondria, inadvertently, disrupting metabolic processes [56, 57], and multiple research investigations have documented ROS-mediated apoptotic responses across several tumor models [57, 58]. If jasmonate-like chemistry was enriched in *L. javanica*, the plant may contribute to cytotoxic effects at elevated concentrations, notwithstanding the net mixture's antioxidative behavior under the experimental conditions employed [35, 36].

The chemistry of *L. javanica* varies by chemotype (piperitenone-, carvone-, linalool, or myrcenone-rich), which can modulate biological effects [59]. The metabolomic analysis confirms the divergence of composition from *A. calamus* and focuses on phenylpropanoid, flavonoid, or jasmonate classes for fractionation [33]. The profile for *A. calamus* inherently invokes concerns pertaining to translation, although β-asarone and some crude extracts have the potential to exhibit antiproliferative activity both *in vitro* and *in vivo* [60–62]. β-asarone has been identified as a carcinogenic and genotoxic component in rodents as well as hepatotoxic in preclinical models; this necessitates the establishment of regulatory limits in phytomedicine as well as food products [62]. Consequently, any trajectory for the development of products must prioritize asarone-depleted fractions or alternatives devoid of asarone if the exploration of efficacy is to be conducted safely [42, 43, 62]. It is crucial to note that putative annotations of mescaline-and steroid-like compounds probable indicate structurally associated plant-derived analogues sharing common triterpenoid or phenethylamine biosynthetic scaffolds, instead of definitive identification of canonical reference molecules [48, 63].

Accordingly, SwissADME analysis was employed to provide functional prioritization of annotated metabolites. The SwissADME software was utilized alongside complementary cheminformatics principles (Lipinski, Veber, Ghose, Egan, Muegge), and in conjunction with gastrointestinal absorption/BBB predictions and alert panels (PAINS, Brenk, lead-likeness), this was done to examine the most discriminative metabolites [64–66]. Compounds such as isopropyl β-glucoside, 6β-hydroxymethandienone, and 7-epi-12-hydroxyjasmonic were identified through the internal ADME heatmap as advantageous lead-like candidates that are grounded in minimal rule infractions, bioavailability assessments, and feasible synthetic accessibility [44]. Although SwissADME's BOILED-Egg framework serves as an ideal tool for preliminary evaluation for BBB and gastrointestinal predictions, further orthogonal verification is usually required through experimental assays such as PAMPA, MDCK/P-gp transport, and microsomal stability as described in this study [47, 67]. Within this limitation-aware framework, *in silico* ADME predictions still serve as a critical early-stage filter for selecting candidate phytometabolites with translational possibility in neuroblastoma research [68]. Predicted BBB permeability is mostly applicable for neuroblastoma, given the connection of paraspinal, intracranial, or central nervous system-adjacent disease locations, where incomplete tissue penetration can restrict therapeutic efficacy [44]. Moreover, predicted P-glycoprotein (P-gp) substrate status alerts the probability of active efflux, which might decrease intracellular accumulation and influence multidrug resistance [69]. Lastly, cytochrome P450 (CYP) inhibition profiles present understanding into possible metabolic liabilities and drug-drug interaction risks, which are important considerations in pediatric oncology settings where integration therapies are common [70]. In general, these parameters reinforce rational prioritization of phytometabolites for downstream optimization, while emphasizing compounds that might need structural refinement or different delivery approaches.

Natural products remain significantly important as complementary or primary scaffolds for neuroblastoma-based therapies, particularly polyphenols, which are a class of

secondary metabolites known to influence apoptosis activity and autophagy, and may also specifically target neuroblastoma stem-like cell populations [71, 72]. A compilation of recent scholarly reviews has systematically outlined a variety of phytochemicals exhibiting preclinical activity against neuroblastoma and highlighted proposed combinations of probable strategies aimed at augmenting responses to standard therapeutic regimens [73]. Within this body of literature, our findings motivate a chemotype-specific follow-up: (i) to deprioritize asarone-rich fractions of *A. calamus* or to specifically eliminate β-asarone before experimental testing due to safety concerns [62], (ii) to assess and evaluate flavonoid conjugates for their potential to modulate redox status and kinase signaling pathways in neuroblastoma [74], and (iii) to extract jasmonate-like metabolites from *L. javanica* for the purpose of investigating the direct targeting of mitochondrial pathways [57].

Together, these results offer a rationale for structured future investigations that incorporate chemotype-informed isolation approaches, bioactivity-guided fractionation, and target-focused mechanistic assessment.

Future directions

Building on potential chemotypic signatures identified by incorporating univariate and multivariate metabolomic analyses, future work should prioritize targeted isolation of potential metabolites from dominant chemical classes. Bioactivity-guided fractionation methods can be critical to connect specific phytochemical fractions to functional effects studies in neuroblastoma cells and to isolate active constituents from complex extract mixtures. In silico structure-based molecular docking and molecular dynamics can be used to screen relevant molecular targets against neuroblastoma. To support rational prioritization of candidate chemotypes and guide hypothesis-driven mechanistic investigations.

Conclusion

This study employed an integrated workflow of untargeted metabolomics, mitochondrial functional assessment, and *in silico* ADME to explore phytometabolites from *L. javanica* and *A. calamus* in human SH-SY5Y neuroblastoma cells. Univariate and multivariate investigations uncovered distinct chemotypic signatures, with *L. javanica* characterized by flavonoid- and polyphenol-enriched profiles and *A. calamus* was dominated by jasmonate-, phenylpropanoid- and lipophilic terpenoid-associated metabolites. Extract exposure related to dose-dependent reductions in cell viability and modulation of mitochondrial membrane potential. In silico pharmacokinetic predictions supported early-stage prioritization of selected chemotypes such as isopropyl β-glucoside, 6β-hydroxymethandienone, and 7-epi-12-hydroxyjasmonic acid. These results are preliminary and hypothesis-generating, and further mechanistic confirmation and *in vivo* studies are recommended to establish biological mechanisms and translational importance.

Author contributions

Conceptualization, MM and NM; methodology, EP, NM, MZ, CO, BI, and MM; software, NM, MZ, BI, and EP; validation, CN, CO, NM, and MM; formal analysis, MM, NM, CN, MZ, and EP; investigation, MM, NM, and CN; resources, EP, MZ, CO, MM, BI, and NM; data curation, NM and MM; writing – original draft preparation, NM and MM; writing – review and editing, MM, CO, BI, EP, MZ, NM, and CN; visualization, MM, NM, BI, and CN; supervision, EP, MZ, CO, MM, BI, and NM; project administration, MM and NM; funding acquisition, MM, CO, and NM. All authors contributed to the article and approved the submitted version.

Data availability

The original contributions presented in the study are included in the article/Supplementary Material, further inquiries can be directed to the corresponding author.

Ethics statement

Ethical approval was not required for the studies on humans in accordance with the local legislation and institutional requirements because only commercially available established cell lines were used.

Funding

The author(s) declared that financial support was received for this work and/or its publication. This research was funded by South Africa's National Research Foundation grant number MND210524603403.

Acknowledgements

Research reported in this publication/article was supported by Sefako Makgatho Health Sciences University. We would also like to sincerely thank the South African Medical Research Council (SAMRC) through its Division of Research Capacity Development under the Research Capacity Development Initiative.

Conflict of interest

The author(s) declared no potential conflicts of interest with respect to the research, authorship, and/or publication of this article.

Generative AI statement

The author(s) declared that generative AI was not used in the creation of this manuscript.

Any alternative text (alt text) provided alongside figures in this article has been generated by Frontiers with the support of artificial intelligence and reasonable efforts have been made to ensure accuracy, including review by the authors wherever possible. If you identify any issues, please contact us.

Supplementary material

The Supplementary Material for this article can be found online at: https://www.ebm-journal.org/articles/10.3389/ebm.2026.10867/full#supplementary-material

References

1. National Cancer Institute. Childhood neuroblastoma treatment (PDQ®)–health professional version (2025). Available online at: https://www.cancer.gov/types/neuroblastoma/hp (Accessed September 12, 2025).

2. D'Ambrosio N, Lyo JK, Young RJ, Haque SS, Karimi S. Imaging of metastatic CNS neuroblastoma. *AJR Am J Roentgenol* (2010) **194**(5):1223–9. doi:10.2214/AJR.09.3203

3. Vo KT, Matthay KK, Neuhaus J, London WB, Hero B, Ambros PF, et al. Clinical, biologic, and prognostic differences on the basis of primary tumor site in neuroblastoma: a report from the international neuroblastoma risk group project. *J Clin Oncol* (2014) **32**(28):3169–76. doi:10.1200/JCO.2013.54.2315

4. Motshudi MC, Naidoo CM, Mkolo NM. The race against time for the enhancement of African national strategic plans in the neuroblastoma research heterogeneity. *Publications* (2024) **12**(4):45. doi:10.3390/publications12040045

5. Davidoff AM. Neuroblastoma. *Semin Pediatr Surg* (2012) **21**(1):2–14. doi:10.1053/j.sempedsurg.2011.10.009

6. Speleman F, Park JR. Henderson TO. Neuroblastoma: a tough nut to crack. *Am Soc Clin Oncol Educ Book* (2016) **35**:548–57. doi:10.1200/EDBK_159169

7. Cohn SL, Pearson ADJ, London WB, Monclair T, Ambros PF, Brodeur GM, et al. The international neuroblastoma risk group (INRG) classification system: an INRG task force report. *J Clin Oncol* (2009) **27**(2):289–97. doi:10.1200/JCO.2008.16.6785

8. Matthay KK, Maris JM, Schleiermacher G, Nakagawara A, Mackall CL, Diller L, et al. Neuroblastoma. *Nat Rev Dis Primers* (2016) **2**:16078. doi:10.1038/nrdp.2016.78

9. Kovalevich J, Langford D. *Considerations for the use of SH-SY5Y neuroblastoma cells in neurobiology*. New Jersey: Humana Press (2013). p. 9–21. doi:10.1007/978-1-62703-640-5_2.18

10. Xicoy H, Wieringa B, Martens GJ. The SH-SY5Y cell line in Parkinson's disease research: a systematic review. *Mol Neurodegener* (2017) **12**(1):10. doi:10.1186/s13024-017-0149-0

11. Shipley MM, Mangold CA, Szpara ML. Differentiation of the SH-SY5Y human neuroblastoma cell line. *J Vis Exp* (2016) **108**:53193. doi:10.3791/53193

12. Engel M, Do-Ha D, Muñoz SS, Ooi L. Common pitfalls of stem cell differentiation: a guide to improving protocols for neurodegenerative disease models and research. *Cell. Mol. Life Sci* (2016) **73**(19):3693–709. doi:10.1007/s00018-016-2265-3

13. Zorov DB, Juhaszova M, Sollott SJ. Mitochondrial reactive oxygen species (ROS) and ROS-induced ROS release. *Physiol Rev* (2014) **94**(3):909–50. doi:10.1152/physrev.00026.2013

14. Fulda S, Galluzzi L, Kroemer G. Targeting mitochondria for cancer therapy. *Nat Rev Drug Discov* (2010) **9**(6):447–64. doi:10.1038/nrd3137

15. Trachootham D, Alexandre J, Huang P. Targeting cancer cells by ROS-mediated mechanisms: a radical therapeutic approach? *Nat Rev Drug Discov* (2009) **8**(7):579–91. doi:10.1038/nrd2803

16. Schumacker PT. Reactive oxygen species in cancer cells: live by the sword, die by the sword. *Cancer Cell* (2006) **10**(3):175–6. doi:10.1016/j.ccr.2006.08.015

17. Selim NA, Wojtovich AP. Mitochondrial membrane potential and compartmentalized signaling: calcium, ROS, and beyond. *Redox Biol* (2025) **86**:103859. doi:10.1016/j.redox.2025.103859

18. Patil GV, Dass SK, Chandra R. *Artemisia afra* and modern diseases. *J Pharmacogenom Pharmacoprot* (2011) **2**(3):2153. doi:10.4172/2153-0645.1000105

19. Motshudi MC, Olaokun OO, Mkolo NM. Evaluation of GC×GC-TOF-MS untargeted metabolomics, cytotoxicity, and antimicrobial activity of leaf extracts of Artemisia afra (Jacq.) purchased from three local vendors. *J King Saud Univ Sci* (2021) **33**(4):101422. doi:10.1016/j.jksus.2021.101422

20. van Wyk BE. The potential of South African plants in the development of new medicinal products. *S Afr J Bot* (2011) **77**(4):812–29. doi:10.1016/j.sajb.2011.08.011

21. Mehrbod P, Abdalla MA, Njoya EM, Ahmed AS, Fotouhi F, Farahmand B, et al. South African medicinal plant extracts active against influenza A virus. *BMC Complement Altern Med* (2018) **18**(1):112. doi:10.1186/s12906-018-2184-y

22. Mkolo NM, Naidoo CM, Kadye R, Obi CL, Iweriebor BC, Olaokun OO, et al. Identification of South African plant-based bioactive compounds as potential inhibitors against the SARS-CoV-2 receptor. *Pharmaceuticals* (2024) **17**(7):821. doi:10.3390/ph17070821

23. Spies L, Koekemoer TC, Sowemimo AA, Goosen ED, Van de Venter M. Caspase-dependent apoptosis induced by *Artemisia afra* Jacq. ex willd in a mitochondria-dependent manner after G2/M arrest. *South Afr J Bot* (2013) **84**:104–9. doi:10.1016/j.sajb.2012.10.007

24. Miraj S, Alesaeidi S. A systematic review study of therapeutic effects of *Matricaria recuitta chamomile* (chamomile). *Electron Physician* (2016) **8**(9):3024–31. doi:10.19082/3024

25. van Loggenberg S, Willers C, van der Kooy F, Gouws C, Hamman JH, Steyn JD. Evaluating *in vitro* cytotoxic effects of *Artemisia afra* and *Artemisia annua* infusions against selected lung cancer cell lines. *South Afr J Bot* (2022) **150**:404–11. doi:10.1016/j.sajb.2022.07.028

26. Sobol Z, Homiski ML, Dickinson DA, Spellman RA, Li D, Scott A, et al. Development and validation of an *in vitro* micronucleus assay platform in TK6 cells. *Mutat Res* (2012) **746**(1):29–34. doi:10.1016/j.mrgentox.2012.02.005

27. Fabre N, Rustan I, de Hoffmann E, Quetin-Leclercq J. Determination of flavone, flavonol, and flavanone aglycones by negative ion liquid chromatography electrospray ion trap mass spectrometry. *J Am Soc Mass Spectrom* (2001) **12**(6):707–15. doi:10.1016/s1044-0305(01)00226-4

28. Liu TY, Tan ZJ, Jiang L, Gu JF, Wu XS, Cao Y, et al. Curcumin induces apoptosis in gallbladder carcinoma cell line GBC-SD cells. *Cancer Cell Int* (2013) **13**(1):64. doi:10.1186/1475-2867-13-64

29. Ru J, Li P, Wang J, Zhou W, Li B, Huang C, et al. TCMSP: a database of systems pharmacology for drug discovery from herbal medicines. *J Cheminform* (2014) **6**(1):13. doi:10.1186/1758-2946-6-13

30. Khan S, Madhi SA, Olwagen C. *In-silico* identification of potential inhibitors against FabI protein in Klebsiella pneumoniae. *J Biomol Struct Dyn* (2024) **42**(3):1506–17. doi:10.1080/07391102.2023.2200571

31. Mwangi JW, Addae-Mensah I, Munavu RM, Lwande W. Essential oils of Kenyan *Lippia* species. Part III. *Flavour Fragr J* (1991) **6**(3):221–4. doi:10.1002/ffj.2730060311

32. Manenzhe NJ, Potgieter N, Van Ree T. Composition and antimicrobial activities of volatile components of *Lippia javanica*. *Phytochemistry* (2004) **65**(16):2333–6. doi:10.1016/j.phytochem.2004.07.020

33. Viljoen AM, Subramoney S, van Vuuren SF, Başer KHC, Demirci B. The composition, geographical variation and antimicrobial activity of *Lippia javanica* (Verbenaceae) leaf essential oils. *J Ethnopharmacol* (2005) **96**(1–2):271–7. doi:10.1016/j.jep.2004.09.017

34. Lukwa N, Mølgaard P, Furu P, Bøgh C. *Lippia javanica* (Burm.f.) Spreng: its general constituents and bioactivity on mosquitoes. *Trop Biomed* (2009) 85–91.

35. Chagonda LS, Chalchat J-C. Essential oil composition of *Lippia javanica* (Burm.f.) Spreng chemotype from Western Zimbabwe. *J Essent Oil Bear Plants* (2015) **18**(2):482–5. doi:10.1080/0972060x.2014.1001140

36. Maroyi A. *Lippia javanica* (Burm.f.) spreng.: traditional and commercial uses and phytochemical and pharmacological significance in the African and Indian subcontinent. *Evid Based Complement Altern Med* (2017) **2017**(1):6746071. doi:10.1155/2017/6746071

37. Muranaka T, Saito K. Production of pharmaceuticals by plant tissue cultures. *Compreh Nat Prod Chem Biol* (2010) **3**:615–28. doi:10.1016/B978-008045382-8.00065-4

38. Sharma V, Sharma R, Gautam DS, Kuca K, Nepovimova E, Martins N. Role of vacha (*Acorus calamus* linn.) in neurological and metabolic disorders: evidence from ethnopharmacology, phytochemistry, pharmacology and clinical study. *J Clin Med* (2020) **9**(4):1176. doi:10.3390/jcm9041176

39. Liu NQ, Van der Kooy F, Verpoorte R. *Artemisia afra*: a potential flagship for African medicinal plants? *S Afr J Bot* (2009) **75**(2):185–95. doi:10.1016/j.sajb.2008.11.001

40. Lang SJ, Schmiech M, Hafner S, Paetz C, Steinborn C, Huber R, et al. Antitumor activity of an *Artemisia annua* herbal preparation and identification of active ingredients. *Phytomedicine* (2019) **62**:152962. doi:10.1016/j.phymed.2019.152962

41. Vogel D, Loots E, Oladimeji O, Gouws C, van der Kooy F. The anti-neoplastic activity of *Artemisia afra* in breast cancer cell lines. *S Afr J Bot* (2023) **157**:115–21. doi:10.1016/j.sajb.2023.03.049

42. Das BK, Swamy AHV, Koti BC, Gadad PC. Experimental evidence for use of *Acorus calamus* (Asarone) for cancer chemoprevention. *Heliyon* (2019) **5**(5):e01585. doi:10.1016/j.heliyon.2019.e01585

43. Yende SR, Harle U, Rajgure DT, Tuse T, Vyawahare NS. Pharmacological profile of *Acorus calamus:* an overview. *Pharmacogn Rev* (2008) **2**(4):23–6.

44. Daina A, Michielin O, Zoete V. SwissADME: a free web tool to evaluate pharmacokinetics, drug-likeness and medicinal chemistry friendliness of small molecules. *Sci Rep* (2017) **7**(1):42717. doi:10.1038/srep42717

45. Djoumbou Feunang Y, Eisner R, Knox C, Chepelev L, Hastings J, Owen G, et al. ClassyFire: automated chemical classification with a comprehensive, computable taxonomy. *J Cheminform* (2016) **8**(1):61. doi:10.1186/s13321-016-0174-y

46. Pires DEV, Blundell TL, Ascher DB. pkCSM: predicting small-molecule pharmacokinetic and toxicity properties using graph-based signatures. *J Med Chem* (2015) **58**(9):4066–72. doi:10.1021/acs.jmedchem.5b00104

47. Daina A, Zoete V. A BOILED-egg to predict gastrointestinal absorption and brain penetration of small molecules. *ChemMedChem* (2016) **11**(11):1117–21. doi:10.1002/cmdc.201600182

48. Sumner LW, Amberg A, Barrett D, Beale MH, Beger R, Daykin CA, et al. Proposed minimum reporting standards for chemical analysis chemical analysis working group (CAWG) metabolomics standards initiative (MSI). *Metabolomics* (2007) **3**:211–21. doi:10.1007/s11306-007-0082-2

49. Thermo Fisher Scientific. *Cell culture basics handbook*. Waltham, MA, USA: Thermo Fisher Scientific (2022). Available online at: https://www.thermofisher.com/cellculturebasics (Accessed September 12, 2025).

50. Dojindo molecular technologies, Inc. 2018. cell counting Kit-8 (CCK-8) protocol (2025). Available online at: https://www.dojindo.com/products/pdf/Protocol/Cell_Counting_Kit-8.pdf (Accessed 12 September, 2025).

51. Sakamuru S, Zhao J, Attene-Ramos MS, Xia M. *Mitochondrial membrane potential assay*. New York: Springer US (2022). p. 11–9. doi:10.1007/978-1-0716-2213-1_2

52. Kopustinskiene DM, Jakstas V, Savickas A, Bernatoniene J. Flavonoids as anticancer agents. *Nutrients* (2020) **12**(2):457. doi:10.3390/nu12020457

53. Newman DJ, Cragg GM. Natural products as sources of new drugs over the nearly four decades from 01/1981 to 09/2019. *J Nat Prod* (2020) **83**(3):770–803. doi:10.1021/acs.jnatprod.9b01285

54. Worley B, Powers R. Multivariate analysis in metabolomics. *Curr Metabolomics* (2013) **1**(1):92–107. doi:10.2174/2213235X11301010092

55. Triba MN, Le Moyec L, Amathieu R, Goossens C, Bouchemal N, Nahon P, et al. PLS/OPLS models in metabolomics: the impact of permutation of dataset rows on the K-fold cross-validation quality parameters. *Mol Biosyst* (2015) **11**(1):13–9. doi:10.1039/C4MB00414K

56. Wishart DS. Emerging applications of metabolomics in drug discovery and precision medicine. *Nat Rev Drug Discov* (2016) **15**(7):473–84. doi:10.1038/nrd2016.32

57. Rotem R, Heyfets A, Fingrut O, Blickstein D, Shaklai M, Fleischer E. Jasmonates: novel anticancer agents acting directly and selectively on human cancer cell mitochondria. *Cancer Res* (2005) **65**(5):1984–93. doi:10.1158/0008-5472.CAN-04-3091

58. Fleischer E. Jasmonates—A new family of anti-cancer agents. *Anticancer Drugs* (2005) **16**(9):911–6. doi:10.1097/01.cad.0000176501.63680.80

59. Fingrut O, Reischer D, Rotem R, Goldin N, Altboum I, Zan-Bar I, et al. Jasmonates induce nonapoptotic death in high-resistance mutant p53-Expressing B-Lymphoma cells. *Br J Pharmacol* (2005) **146**(6):800–8. doi:10.1038/sj.bjp.0706394

60. Mujovo SF, Hussein AA, Meyer JJ, Fourie B, Muthivhi T, Lall N. Bioactive compounds from *Lippia javanica* and *Hoslundia opposita*. *Nat Prod Res* (2008) **22**(12):1047–54. doi:10.1080/14786410802250037

61. Mukherjee PK, Kumar V, Mal M, Houghton P. *Acorus Calamus*: scientific validation of ayurvedic tradition from natural resources. *Pharm Biol* (2008) **45**(8):651–66. doi:10.1080/13880200701538724

62. Hasheminejad G, Caldwell J. Genotoxicity of the alkenylbenzenes α– and β-asarone, myristicin and elemicin as determined by the UDS assay in cultured rat hepatocytes. *Mutat Res* (1994) **321**(3):89–97. doi:10.1016/0278-6915(94)90194-5

63. Facchini FPJ. Alkaloid biosynthesis in plants: biochemistry, cell biology, molecular regulation, and metabolic engineering applications. *Annu Rev Plant Physiol Plant Mol Biol* (2001) **52**:29–66. doi:10.1146/annurev.arplant.52.1.29

64. Thimmappa R, Geisler K, Louveau T, O'Maille P, Osbourn A. Triterpene biosynthesis in plants. *Annu Rev Plant Biol* (2014) **65**:225–57. doi:10.1146/annurev-arplant-050312-120229

65. Lipinski CA, Lombardo F, Dominy BW, Feeney PJ. Experimental and computational approaches to estimate solubility and permeability in drug discovery and development settings. *Adv Drug Deliv Rev* (1997) **23**(1–3):3–25. doi:10.1016/S0169-409X(96)00423-1

66. Brenk R, Schipani A, James D, Krasowski A, Gilbert IH, Frearson J, et al. Lessons learnt from assembling screening libraries for drug discovery for neglected diseases. *ChemMedChem* (2008) **3**(3):435–44. doi:10.1002/cmdc.200700139

67. Avdeef AADrug Development. *Solubility, permeability, and charge state*. 2nd ed. New Jersey: John Wiley and Sons (2012). doi:10.1002/9781118286067#:~:text=10.1002/9781118286067

68. Pardridge WM. The blood-brain barrier: bottleneck in brain drug development. *NeuroRx* (2005) **2**(1):3–14. doi:10.1602/neurorx.2.1.3

69. Gottesman MM, Fojo T, Bates SE. Multidrug resistance in cancer: role of ATP-dependent transporters. *Nat Rev Cancer* (2002) **2**(1):48–58. doi:10.1038/nrc706

70. Zhou SF. Drugs behave as substrates, inhibitors and inducers of human cytochrome P450 3A4. *Curr Drug Metab* (2008) **9**(4):310–22. doi:10.2174/138920008784220664

71. Hill A, Gupta R, Zhao D, Vankina R, Amanam I, Salgia R. Targeted therapies in non-small-cell lung cancer. *Precision Medicine Cancer Therapy* (2019) **178**, 3–43. doi:10.1007/978-3-030-16391-4_1

72. Li Y, Liu T, Ivan C, Huang J, Shen D-Y, Kavanagh JJ, et al. Corrigendum: enhanced cytotoxic effects of combined valproic acid and the Aurora kinase inhibitor VE465 on gynecologic cancer cells. *Front Oncol* (2018) **8**:9. doi:10.3389/fonc.2018.00009

73. Cheung NKV, Dyer MA. Neuroblastoma: developmental biology, cancer genomics, and immunotherapy. *Nat Rev Cancer* (2013) **13**(6):515–34. doi:10.1038/nrc3526

74. Wang K, Zhang T, Dong Q, Nice EC, Huang C, Wei Y. Redox homeostasis: the linchpin in stem cell self-renewal and differentiation. *Cell Death Dis* (2013) **4**(3):e537. doi:10.1038/cddis.2013.50